EBioMedicine 52 (2020) 102637

Contents lists available at ScienceDirect

EBioMedicine

journal homepage: www.elsevier.com/locate/ebiom

Research paper

Canagliflozin impairs blood reperfusion of ischaemic lower limb partially by inhibiting the retention and paracrine function of bone marrow derived mesenchymal stem cells

Yinuo Lin[a,#], Jinliang Nan[b,#], Jian Shen[b,#], Xinhuang Lv[c,#], Xiao Chen[a], Xingmei Lu[d], Chi Zhang[b], Pingping Xiang[b], Zhiting Wang[a,**], Zhengzheng Li[c,*]

[a] Wenzhou Municipal Key Cardiovascular Research Laboratory, Department of Cardiology, The First Affiliated Hospital, Wenzhou Medical University, Wenzhou 325000, Zhejiang Province, China
[b] Provincial Key Cardiovascular Research Laboratory, Department of Cardiology, The Second Affiliated Hospital, Zhejiang University School of Medicine, Hangzhou 310009, Zhejiang Province, China
[c] Research Institute of Experimental Neurobiology, Department of Neurology, The First Affiliated Hospital, Wenzhou Medical University, Wenzhou 325000, Zhejiang Province, China
[d] Department of Pathology, The First Affiliated Hospital, Wenzhou Medical University, Wenzhou 325000, Zhejiang Province, China

ARTICLE INFO

Article History:
Received 11 August 2019
Revised 16 December 2019
Accepted 8 January 2020
Available online xxx

Keywords:
Canagliflozin
Mesenchymal Stem Cells
Mitochondria
Glutamate dehydrogenase
Ischaemia

ABSTRACT

Background: Canagliflozin (CANA) administration increases the risk of lower limb amputation in the clinic. The present study aimed to investigate whether and how CANA interferes with the intracellular physiological processes of bone marrow derived mesenchymal stem cells (BM-MSCs) and its contribution to ischaemic lower limb.
Methods: The *in vivo* blood flow recovery in ischaemic lower limbs following CANA treatment was evaluated. The cellular function of BM-MSCs after CANA treatment were also assessed *in vitro*. *In silico* docking analysis and mutant substitution assay were conducted to confirm the interaction of CANA with glutamate dehydrogenase 1 (GDH1).
Findings: Following CANA treatment, attenuated angiogenesis and hampered blood flow recovery in the ischaemic region were detected in diabetic and non-diabetic mice, and inhibition of the proliferation and migration of BM-MSCs were also observed. CANA was involved in mitochondrial respiratory malfunction in BM-MSCs and the inhibition of ATP production, cytochrome c release and vessel endothelial growth factor A (VEGFA) secretion, which may contribute to reductions in the tissue repair capacity of BM-MSCs. The detrimental effects of CANA on MSCs result from the inhibition of GDH1 by CANA (evidenced by *in silico* docking analysis and H199A-GDH1/N392A-GDH1 mutant substitution).
Interpretation: Our work highlights that the inhibition of GDH1 activity by CANA interferes with the metabolic activity of the mitochondria, and this interference deteriorates the retention of and VEGFA secretion by MSCs.
Funding: National Natural Science Foundation of China, Natural Science Foundation of Zhejiang Province and Wenzhou Science and Technology Bureau Foundation.

1. Introduction

Sodium-glucose cotransporter 2 inhibitors (SGLT2is) are a new class of oral antidiabetic drugs that inhibit sodium-glucose cotransporter 2, which functions as the main glucose transporter of the kidney and is responsible for the reabsorption of 90% of glucose from primary urine. A SGLT2i reduces the reabsorption of glucose in convoluted proximal tubules and therefore enhances urinary glucose excretion, which consequently decreases both fasting and postprandial hyperglycaemia. Meta-analyses of clinical trials of type 2 diabetes have indicated that either SGLT2i monotherapy or SGLT2i combined with other hypoglycaemic agents all reduce the fasting plasma glucose, hemoglobin A1c (HbA1c), and body weight [1–3]. Interestingly, recent clinical trials have shown that although the difference in HbA1c between randomized groups was comparable, SGLT2is reduce cardiovascular disease and cardiovascular mortality in patients with type 2 diabetes mellitus (T2DM) compared with the results obtained

* Corresponding author.
** Co-corresponding author Wenzhou Municipal Key Cardiovascular Research Laboratory, Department of Cardiology, The First Affiliated Hospital, Wenzhou Medical University, Wenzhou 325000, Zhejiang Province, China.
E-mail addresses: wzt665523@sina.com (Z. Wang), Leezz2005@126.com (Z. Li).
# These four authors contributed equally to the manuscript.

https://doi.org/10.1016/j.ebiom.2020.102637

Research in context

Evidence before this study

Several clinical trials have indicated that the use of canagliflozin, a new class of oral antidiabetic drugs that inhibit sodium-glucose cotransporter 2, increases the risk of lower extremity amputation. Canagliflozin has also been found to serve as an inhibitor of endothelial cell proliferation and tube formation and might both induce worsening of preexisting peripheral artery disease and cause lower extremity ischaemia. Bone marrow derived mesenchymal stem cells play important roles during the rescue and repair of ischaemic organs and tissues. Notably, mesenchymal stem cells are also involved in the process of tissue repair and regeneration in acute and chronic skeletal muscle damage.

We searched articles published in PubMed until August 1st, 2019, without language restrictions. We used the terms ("canagliflozin") AND ("mesenchymal stem cell" OR "mesenchymal stromal cell") AND ("limb ischaemia" OR "limb ischaemia"). No previous study reporting the effect of canagliflozin on bone marrow derived mesenchymal stem cells has been published.

Added value of this study

To our knowledge, this study constitutes the first investigation specifically designed to evaluate the effect of canagliflozin on bone marrow derived mesenchymal stem cells. Our study indicates that canagliflozin impairs the biological function of bone marrow derived mesenchymal stem cells and thus may hinder blood flow recovery in ischaemic lower limb. These effects of canagliflozin are mediated through inhibition of the tricarboxylic acid cycle, which occurs through the direct interaction of canagliflozin with hexamer of glutamate dehydrogenase 1 and the subsequent inhibition of the activity of this enzyme, and these effects reduce the production of ATP and disrupt mitochondrial homeostasis. These findings suggest an off-target adverse effect of canagliflozin that is independent of the inhibition of sodium-glucose cotransporter 2.

Implications of all the available evidence

Amputation has a large negative impact on the clinical course of diabetic patients. Our study may provide a novel explanation for the canagliflozin-induced increase in amputation risk in patients with prior amputations and/or the presence of peripheral artery disease and suggests that a refined therapeutic strategy for canagliflozin is urgently required for these patients. Additionally, our findings might also provide evidence supporting the application of canagliflozin in some new indications, such as anti-tumor therapy.

with other glucose-lowering drugs [4–6], which implies involvement of the pleiotropic effects of these agents.

Conversely, due to their unique mode of action, SGLT2is have several characteristic adverse effects, such as hypoglycaemia and genital and urinary tract infections. However, the CANVAS program reported an unexpected increase (approximately twofold) in the risk of lower extremity amputation in the canagliflozin (CANA)-treated group, with the majority of amputations occurring at the toe and transmetatarsal levels [7]. A recent pharmacovigilance analysis suggested that compared with empagliflozin and dapagliflozin (DAPA), CANA is associated with a higher risk of amputation [8]. In contrast, a subanalysis of the large-scale cardiovascular outcome trial EMPA-REG OUTCOME revealed that the SGLT2i empagliflozin prevents the need for amputations, even among participants with a history of peripheral artery disease [4]. It has been speculated that the increased risk of amputation might be attributed to changes in limb blood flow that deteriorate with peripheral artery disease. However, no mechanistic and preclinical investigations have addressed this speculation.

Bone marrow derived mesenchymal stem cells (BM-MSCs) constitute a population of multipotential cells that can be differentiated into adipocyte, osteoblast, chondrocyte, and endothelial lineages. During organ injury, BM-MSCs can be mobilized to peripheral blood under hypoxic stress [9], migrate to injured tissues [10,11] and exert protective effects. Thus, BM-MSCs play important roles during the rescue and repair of ischaemic organs and tissues. Notably, MSCs are also involved in the process of tissue repair and regeneration in acute and chronic skeletal muscle damage [12,13].

The conversion of glutamate into α-ketoglutarate (anaplerosis) can be mediated by glutamate dehydrogenase 1 (GDH1), which plays a key role in glutamine anaplerosis. Hence, the catalytic process elicited by GDH1 produces adequate alpha-ketoglutarate (α-KG), an important intermediate in the tricarboxylic acid (TCA) cycle, which is a prerequisite for increasing the intra-mitochondrial NADH/NAD+ ratio and generating the proton gradient needed for ATP production. CANA inhibits the activity of the TCA cycle, and this affect might be achieved through the inhibition of GDH1 [14]. However, the previous studies show a lack of causal reasoning. Thus, molecular docking analysis and GDH1 mutagenesis were employed to illustrate the role of CANA in the inhibition of GDH1 in our study.

Thus far, the effect of CANA on BM-MSCs has not been explored. Therefore, this study constitutes the investigation aiming to determine the main mechanism through which CANA inhibits the TCA cycle. This was achieved by illustrating the specific drug target in GDH1 that results in impairment of the biological and paracrine functions of MSCs, which may ultimately affects blood reperfusion recovery in ischaemic skeletal muscles.

2. Materials and methods

2.1. Cell lines, culture conditions and treatments

Mouse BM-MSCs were purchased from Cyagen Biosciences (Guangzhou, China), and human umbilical vein endothelial cells (HUVECs) were purchased from ScienCell (CA, USA). HUVECs were cultured in M199 media (Gibco, USA), and BM-MSCs were cultured in Dulbecco's modified Eagle's medium (DMEM, Corning, USA). The culture medium was supplemented with 10% (v/v) FBS, 100 U/mL penicillin and 100 μg/mL streptomycin (HyClone, USA). All cells were maintained at 37 °C in a 5% CO_2 incubator. BM-MSCs were treated with 5 or 10 μM CANA (Apexbio, USA) or 10 μM DAPA (Apexbio, USA), and 0.1% dimethyl sulfoxide (DMSO) was used as a negative control. The compound structures of CANA and DAPA are shown in Supplementary Fig. I. Working solutions were prepared in DMEM supplemented with 2% (v/v) FBS, and the vehicle (DMSO) constituted no more than 0.1% (v/v) of the medium.

2.2. Cell proliferation assay

Cells were seeded at a density of 1000–2000 cells/well in 96-well plates and treated as indicated in quintuplicate for 48–72 h. Then, 10 μL of cell counting kit-8 (CCK8, Dojindo, Japan) reagent was added to each well and incubated for 2 h at 37 °C, and the absorbance was measured at a wavelength of 450 nm. Cell proliferation was also analysed using a 5-ethynyl-2′-deoxyuridine (EdU) Cell Proliferation Assay Kit (RiboBio, Guangzhou, China) according to the manufacturer's instructions.

2.3. Cell cycle analysis

Cells were harvested and washed twice in PBS at room temperature and resuspended at a concentration of 1×10^6 cells/mL in PBS. For propidium iodide (PI) staining, the washed cells were fixed in

pure ethanol at −20 °C overnight, and the rest of the steps were performed based on the manufacturer's instructions (Beyotime, Beijing, China) followed by analysis using a fluorescence activated cell sorting (FACS) flow cytometer (BD Biosciences, USA).

2.4. Cell apoptosis analysis

The cell apoptosis rate was determined by a FITC-Annexin V Apoptosis Detection Kit (Dojindo, Japan) using flow cytometry according to the manufacturer's instructions. Briefly, cells were detached and washed twice with PBS, resuspended in 300 μL of binding buffer containing 5 μL of FITC-Annexin V and 5 μL of PI, and incubated at room temperature for 20 min. The fluorescence intensity was measured using a FACS flow cytometer (BD Biosciences, USA).

2.5. Cell migration analysis

The cell migration ability was assessed by Transwell migration and wound healing assays. For the Transwell migration assay, BM-MSCs treated with either 10 μM CANA, 10 μM DAPA, or 0.1% (v/v) DMSO (as a negative control) for 48 h were suspended in serum-free medium at a concentration of 5×10^4 cells/mL. A 200-μL cell suspension (1×10^4 cells) was pipetted into the upper chamber. DMEM with 10% foetal bovine serum was added to the lower chamber as a chemoattractant. BM-MSCs were incubated for 24 h at 37 °C, and the cells on the upper side of the membrane were then removed with a cotton swab. The cells that migrated to the lower surface were fixed with 4% paraformaldehyde, stained with 4′,6-diamidino-2-phenylindole (DAPI) or 0.1% crystal violet, and observed using an inverted fluorescence microscope (Leica, Germany) or inverted microscope (Olympus, Japan). For the wound healing assay, BM-MSCs were cultured in 12-well plates, treated as indicated for 48 h, and allowed to grow to confluence. Linear wounds were made with a sterile 200-μL pipette tip. The cells were washed to remove debris using PBS and incubated in serum-free DMEM at 37 °C for 72 h. Serial images of cell migration at 0, 24, 48 and 72 h after scratching were obtained using an inverted microscope (Olympus, Japan). The percentage of closure of the wounded areas at 72 h was calculated as the 72-h migration ratio.

2.6. Western blot analysis

Cell lysates were prepared using radioimmunoprecipitation assay (RIPA) buffer. The samples were separated by SDS-PAGE, transferred to a polyvinylidene fluoride membrane, and immunoblotted with the following antibodies: acetyl coenzyme A carboxylase (ACC, Ab45174, Abcam), phospho-ACC (Ser79) (Ab68191, Abcam), sodium-coupled glucose cotransporter 2 (SGLT2, ab37296, Abcam), adenosine monophosphate activated protein kinase α (AMPKα, CST5832, Cell Signaling Technology), phospho-AMPKα (Thr172) (CST50081, Cell Signaling Technology), cyclin A2 (CCNA2, ET1612-26, Huabio, China), cyclin D1 (CCND1, ET1601-31, Huabio, China), cleaved caspase-3 (CST9661, Cell Signaling Technology), and GDH1 (ab166618, Abcam). After incubation of the membranes with peroxidase-conjugated secondary antibodies (Cell Signaling Technology), bands were visualized using enhanced chemiluminescence reagents (Bio-Rad, USA).

2.7. ATP quantification

BM-MSCs were treated as indicated for 48 h in 12-well plates and then detached using 0.25% trypsin, and 3×10^5 cells were collected for further analysis. ATP production was detected using an Enhanced ATP Assay Kit (Beyotime, China) according to the manufacturer's instructions and visualized by a luminometer (SpectraMax M5, Molecular Devices, USA).

2.8. Oxygen consumption rate analysis

BM-MSCs were cultured in 10-cm dishes and treated with 10 μM CANA, 10 μM DAPA or 0.1% DMSO for 48 h. The BM-MSCs were then detached, and 1×10^6 cells were collected for oxygen consumption rate analysis. An Oxygraph-2k (O2k; OROBOROS Instruments, Innsbruck, Austria) was used to measure respiration in intact cells. A total of 1×10^6 cells were suspended in DMEM (containing 2% FBS), and 2 mL of the cell suspension was then added to the chamber (37 °C). The basal oxygen consumption rate (OCR) of the cells was measured in DMEM with no stimulation, and the maximum OCR of the cells was measured in DMEM after adding 1 μM carbonyl cyanide m-chlorophenylhydrazone (CCCP).

2.9. Transmission electron microscopy (TEM) analysis

Samples were collected and immediately fixed overnight in 2.5% glutaraldehyde. The samples were then rinsed three times with PBS and postfixed with 1% osmic acid for 2 h. After three rinses with deionized water and serial dehydration with 50, 70, 80, 90 and 100% alcohol and 100% acetone, the samples were embedded in epoxy resin to produce blocks of cells. Ultrathin sections (50 nm) were obtained by an ultramicrotome (Ultracut UCT, Leica, Germany). Then, the sections were stained with lead citrate and uranyl acetate and analysed by TEM (T10, FEI, USA).

2.10. Exosome isolation

First, conditioned media (CM) was prepared by incubating BM-MSCs grown to subconfluence in growth media containing 2% exosome-depleted FBS (prepared by overnight ultracentrifugation at 110,000 × *g* and 4 °C) and 10 μM CANA or 0.1% DMSO (as a negative control) for 48 h. Then, the BM-MSCs were detached, and the cell number was counted. The CM was collected and centrifuged at 300 × *g* for 10 min, 2000 × *g* for 10 min and 10,000 g for 30 min to remove cells and cell debris. The supernatant was filtered by a 0.22-μM filter (Millipore, USA) followed by ultracentrifugation at 110,000 × *g* for 70 min (Optima L-90 K; Beckman Coulter, USA). Exosomes were collected and washed once with PBS and centrifugation at 110,000 g for 70 min followed by resuspension in 20 μL of PBS. The protein content of the concentrated exosomes was determined using a bicinchoninic acid (BCA) protein assay kit.

2.11. Conditioned medium preparation and analysis of vegfa secretion

First, BM-MSCs were treated with 0.1% DMSO or 10 μM CANA for 48 h, detached by 0.25% trypsin and suspended in 2 mL of M199 supplemented with 2% FBS at a concentration of 2×10^5 cells/mL. The cells were then plated in six-well culture plates and cultured for an additional 24 h, and the supernatants were collected as conditioned medium. For the analysis of VEGFA secretion, 100 μL of each conditioned medium was transferred to a microcentrifuge tube and centrifuged (3000 × *g*, 20 min, 4 °C), and the concentration of VEGFA in the supernatant was analysed using an enzyme-linked immunosorbent assay (ELISA, USCN, Wuhan, China) according to the manufacturer's instructions.

2.12. Endothelial tube formation assay

The endothelial tube formation assay was performed according to the manufacturer's protocol. Fifty microliters of Matrigel (BD Biosciences, USA) was added to each well of a 96-well plate and allowed to polymerize. HUVECs (2×10^4 cells) were suspended in conditioned medium as mentioned above or M199 containing 2% FBS (as a negative control) and plated on Matrigel. After incubation for 8 h at 37 °C, the cells were observed under an inverted phase contrast microscope

(Olympus, Japan) and imaged. The tube length was measured with Image-Pro-Plus software.

2.13. In silico *docking simulation analysis of cana with GDH1*

The molecular docking procedures were implemented using Molecular Operating Environment (MOE, Chemical Computing Group, Quebec, Canada) software. The three-dimensional (3D) model of the structure of CANA was downloaded from PubChem Compound. The force field was set to MMFF94x, and the partial charges of the models were fixed on the Potential Setup module. The Energy Minimize module was used for the optimization of all atoms (RMSgradient, 0.001 kcal/mol/A2). The refined CANA structure was then saved in the .mdb database for molecular docking analysis.

The protein structure of hexamer of GDH1 was obtained by homology modeling using the Swiss-model homology modeling server (http://swissmodel.expasy.org/). Prior to the docking simulation, the 3D structure model of GDH1 was prepared using the following steps: (i) hydrogen atoms were added to the structures with a standard geometry; (ii) the structure was protonated using Protonate3D; (iii) the structure was minimized using an AMBER10: EHT force-field; and (iv) MOE Alpha Site Finder was used for searching the active site within the enzyme structure, and dummy atoms were created from the obtained alpha spheres.

After the structures of CANA and GDH1 were prepared, MOE Dock was used for docking simulations between CANA and GDH1. The docking workflow followed the "induced fit" protocol, in which the side chains of the receptor pocket were allowed to move according to the ligand conformations but with a constraint on their positions. The weight used for tethering side chain atoms to their initial positions was 10. At first, the docked poses of the ligands were ranked based on London dG scoring. The top five poses were then subjected to force field refinement followed by GBVI/WSA dG rescoring. The docking score and ligand interaction between CANA and GDH1 were obtained.

2.14. *Spectrophotometric kinetic analysis*

The GDH1 enzymatic activity was analysed using a GDH activity assay kit (Solarbio, Beijing, China) according to the manufacturer's instructions, and the decrease in coenzyme absorption at 340 nm was observed at 37 °C using a Beckman Coulter DU-730 spectrophotometer equipped with a Beckman Coulter temperature controller.

2.15. *Construction of and infection with recombinant virus vectors*

Recombinant lentiviruses expressing mouse VEGFA and mouse GDH1 (including the WT, H199A mutant and N392A mutant GDH1) cDNA and lentiviruses carrying shRNAs against the GDH1 gene (shRNA targeting sequence, 5′-GCTCACAGCCGACTTCTTTAC-3′) were all provided by RiboBio. Lentiviruses containing empty plasmids and lentiviruses containing non-specific shRNAs served as controls (CTRLs). BM-MSCs were infected with the purified lentiviruses at multiplicities of infection (MOI) of 10 combined with polybrene (Sigma, USA) at a final concentration of 8 μg/ml. The day after infection, the infection medium was BM-MSC replaced with fresh medium, and the expression of the indicated genes and proteins was determined by PCR, Western blotting or ELISA.

2.16. *Animal model*

All animal experimental protocols were approved by the Animal Care and Use Committee of Wenzhou Medical University. To establish the diabetic mice model, male C57BL/6 mice (aged 6 weeks, weighing 18−20 g) were fed a high-fat diet (HFD; 60 kcal%; Biotech Co. Ltd., Beijing, China) for 4 weeks. After this period of feeding, the average weight of the obese mice was 27 g, and their average blood glucose level was 14.5 mmol/L. Experimental diabetes was then induced by daily intra-peritoneal injections of streptozotocin (STZ; 30 mg/kg, Sigma-Aldrich, St. Louis, MO, USA) in citrate buffer for 4 days. Stable blood glucose levels exceeding 13.78 mmol/l (250 mg/dl) were considered to indicate a diabetic mouse.

For the assessment of vascular regeneration during hindlimb ischaemia, CANA (10 mg/kg/day; n = 6), DAPA (1 mg/kg/day; n = 6) or vehicle control (distilled water containing 0.5% carboxymethyl cellulose and 0.25% Tween-80; n = 6) was administered to diabetic or non-diabetic male C57BL/6 mice (aged 8 weeks, weighing 19−22 g) via oral gavage daily for 28 days. The systolic, diastolic and mean blood pressure, as well as the heart rate were measured with a programmable sphygmomanometer (BP-2010; Softron, Japan) using the tail-cuff method (Softron, Japan). On the 7th day of oral gavage (D 0), ligation and excision of a 3- to 5-mm segment of the femoral artery proximal to the superficial caudal epigastric artery branch was performed, and laser Doppler perfusion imaging (LDPI, PeriCam PSI, Perimed AB, Sweden) was carried out on days 0, 3, 7, 14 and 21 following surgery. The results are presented as the ratios of the ischaemic (right) limb blood flow to the nonischaemic (left) limb blood flow. The mice were sacrificed 21 days after surgery, and their gastrocnemius muscles were collected for further analysis. Serum biological markers and urine glucose levels were measured using routine laboratory methods.

2.17. *Serum analysis of biochemical parameters*

Blood was drawn once from the facial vein before the administration of CANA and DAPA and once by heart puncture after the mice were sacrificed. The serum glucose, alanine transaminase (ALT), aspartate transaminase (AST), blood urea nitrogen (BUN), creatinine (CREA), cholesterol (CHO), and triglyceride (TG) levels were tested using an IDEXX catalyst one® autoanalyser (IDEXX Lab, Westbrook, ME, USA).

2.18. *BM-MSC retention and tissue repair in ischaemic muscle*

For the quantification of BM-MSC retention and tissue repair in ischaemic muscle, parental BM-MSCs were first infected with lentivirus containing luciferase or VEGFA to generate stably transfected cell lines (Luc-MSCs and $MSCs^{VEGFA}$). Luc-MSCs (1×10^6 cells) that were either treated (n = 6) or not treated (n = 6) with 10 μM CANA for 48 h were suspended in 50 μL of PBS and injected into the gastrocnemius muscle at five points with a 50-μL microsyringe 1 h after right iliac artery ligation (IAL). PBS was used as a negative control (n = 5). Bioluminescence imaging (BLI) was performed using a Xenogen system (IVIS Spectrum, Perkin Elmer, USA) at 3 h and 3, 5, and 7 days following surgery. For the evaluation of tissue repair in ischaemic muscle, $MSCs^{VEGFA}$ (n = 6) or MSCs infected with lentivirus containing empty plasmids (MSC^{CTRL}, as control, n = 6) and treated with 10 μM CANA for 48 h were injected into the gastrocnemius muscle as described previously. $MSCs^{CTRL}$ treated with DMSO were used as a positive control (n = 6). LDPI was performed on days 0, 3, 7, 14 and 21 following surgery. The mice were sacrificed on day 21, and their gastrocnemius muscles were collected for further histological analysis.

2.19. *Isolation and culture of BM-MSCs*

BM-MSCs were obtained from the above-mentioned diabetic or non-diabetic mice after the administration of CANA, DAPA or vehicle control for 28 days. Briefly, intact femurs and tibias were collected separately from each mouse and washed several times with PBS containing 500 U/mL penicillin and 500 U/mL streptomycin. Both ends of the femurs and tibias were cut off, and the resulting cavities were flushed with PBS to obtain the bone marrow cells. After centrifugation at 800 rpm for 5 min, the cells (approximately 1×10^8) were resuspended with 5 mL of DMEM/F12 culture medium (Corning, USA) supplemented with 10% FBS, 100 U/mL penicillin, and 100 U/mL

streptomycin and cultured in a T25 flask. The culture medium was replaced after 24 h and changed every other day. The colony numbers and diameters of each flask were obtained after 7 days of culture.

2.20. Histological analysis

The mice were sacrificed 21 days after surgery, and their gastrocnemius muscles were harvested and embedded in optimal cutting temperature compound (Sakura; Torrance, USA). Frozen sections were cut at a 5-μm thickness. To examine the capillary and arteriole densities in ischaemic muscles, the sections were stained with rat anti-mouse CD31 (550274, BD Bioscience, USA) and rabbit anti-mouse smooth muscle α-actin (α-SMA) (ab5694, Abcam) primary antibodies. The sections were further stained with Alexa Fluor 488- and Alexa Fluor 549-conjugated secondary antibodies (Invitrogen, USA) and were analysed using a laser confocal scanning microscope (TCS-SP8, Leica, Germany). The results are presented as arterioles/field and capillaries/field. For morphometric analysis, cryosections of the ischaemic limbs were stained with haematoxylin and eosin (H&E).

2.21. Statistical analysis

All the data are presented as the means ± SDs. Statistical analyses were performed using Prism 6 software (GraphPad Software Inc., USA). Student's *t*-test was performed for comparisons between two groups, and ANOVA followed by Dunnett's correction was used for comparisons between more than two groups. $P<0.05$ was considered statistically significant.

3. Results

3.1. CANA attenuated angiogenesis and blood reperfusion in the ischaemic lower limb

We first evaluated the effect of CANA on ischaemic lower limb angiogenesis in diabetic mice. The general study design was depicted in Supplementary Fig. IIa. The heart rate, blood pressure, as well as the body weight of the diabetic mice administered with CANA and DAPA were comparable to those of the mice administered the vehicle control. However, CANA and DAPA showed a trend in decreasing the body weight of the diabetic mice (Supplementary Fig. IIb~IId). CANA and DAPA also induced decreases in the blood glucose in the diabetic mice within 28 days from the onset of oral drug administration (14.3 ± 0.6 mmol/L vehicle control, 12.0 ± 1.0 mmol/L CANA and 11.9 ± 1.0 mmol/L DAPA, $P<0.05$, means ± SDs) (Supplementary Fig. IIe). We also noted that both CANA and DAPA lowered the serum CHO level without affecting the other blood biochemistry parameters (Supplementary Fig. IIf). However, LDPI revealed that CANA treatment hindered the recovery of perfusion in the diabetic mice at days 14 and 21 compared with the results observed in DAPA- and vehicle control-administered diabetic mice (Fig. 1a, 1b). The capillary and arteriole densities in ischaemic muscles were then analysed by CD31 and smooth muscle α-actin (α-SMA) immunostaining, respectively. In line with the LDPI findings, both the capillary and arteriole densities at day 21 were lower in the mice administered CANA than in those administered the vehicle control (Fig. 1c, 1d and Supplementary Fig. IIIa & IIIb).

BM-MSCs constitute a population of multipotential cells that are involved in the processes of angiogenesis [15,16] and tissue repair and regeneration in acute and chronic skeletal muscle damage [12,17]. Therefore, based on previous findings, we speculated that the endogenous BM-MSC functions might be attenuated by CANA treatment. We isolated BM-MSCs and tested their colony-forming abilities as a parameter of the endogenous BM-MSC functions. The average colony numbers (Fig. 1e, Supplementary Fig. IIIc) and colony diameter (Fig. 1f) obtained with the BM-MSCs from the diabetic mice administered CANA were lower than those obtained with the BM-MSCs obtained from the mice administered the other two treatments.

We also performed the same observations in non-diabetic mice. General study design was depicted in Supplementary Fig. IVa. Neither CANA nor DAPA administration affected the heart rate or blood pressure of normoglycemic C57 mice. Interestingly, The CANA-administered mice exhibited similar increases in the body weights as the DAPA- and vehicle control-administered mice (Supplementary Fig. IVb). In addition, CANA and DAPA administration did not affect the levels of serum glucose in the non-diabetic mice (Supplementary Fig. IVe) but markedly increased the levels of urine glucose (Supplementary Fig. IVf). The blood biochemistry results also showed comparable values of the ALT, AST, BUN, CREA, TG indexes but differences in the CHO levels (Supplementary Fig. IVg). The CANA-administered mice subjected to femoral artery ligation (FAL) surgery exhibited decreased blood reperfusion at days 3, 14 and 21 than the DAPA and vehicle control-administered mice (Fig. 1g&h). A histological analysis indicated that the capillary and arteriole densities at day 21 (Fig. 1i&j; Supplementary Fig. Va & Vb) were lower in the mice administered CANA than in those administered DAPA and the vehicle control. In addition, the average colony numbers (Fig. 1k, Supplementary Fig. Vc) and colony diameter (Fig. 1l) obtained with the BM-MSCs from the normoglycemic mice administered CANA were lower than those obtained with the BM-MSCs obtained from the mice administered the other two treatments.

3.2. BM-MSCs treated with cana exhibited reduced proliferation

Based on the aforementioned results, we inferred that CANA might interfere with the function of BM-MSCs to decrease angiogenesis following FAL surgery. First, the CANA-treated group exhibited significant inhibition of proliferation in culture media containing 2% FBS, whereas the inhibition of proliferation was not strong if the culture medium was supplemented with 5 or 10% FBS (Supplementary Fig. Via&b). Therefore, in the following experiments, culture medium containing 2% FBS was used to assess the effects of CANA on BM-MSCs. The level of cell proliferation, which was assessed by the CCK-8 assay, was decreased by approximately 7% and 18% if the cells were preconditioned with 5 and 10 μM CANA for 48 h and by approximately 11% and 20% if the cells were preconditioned with 5 and 10 μM CANA for 72 h, respectively (Fig. 2a). However, cell proliferation was not affected by DAPA (Fig. 2b). The cell cycle of CANA-treated BM-MSCs was then analysed. Interestingly, the percentage of 5 μM CANA-treated BM-MSCs in S phase was 6.2%, lower than that of untreated BM-MSCs (17.6%), and the percentage further decreased to 5.5% after treatment with 10 μM CANA (Fig. 2c). In addition, the percentage of EdU-stained cells was also significantly reduced by CANA treatment in a dose-dependent manner (10.8% with 5 μM CANA and 7.9% with 10 μM CANA) compared with that found in untreated BM-MSCs (16.7%) (Fig. 2d). AMPK activation is associated with cell cycle arrest, and CANA has been proven to phosphorylate the AMPK (Thr172)/ACC (Ser79) pathway to inhibit the growth of cancer cells [18]. We inferred that inhibited proliferation of BM-MSCs might be caused by phosphorylation of the AMPK (Thr172)/ACC (Ser79) pathway after CANA treatment. As expected, CANA significantly and persistently increased the phosphorylation of AMPK (Thr172) and subsequently phosphorylated ACC (Ser79), which is downstream of the pathway (Fig. 2e). Moreover, CANA treatment markedly reduced the expression level of CCND1 but did not affect the protein expression levels of CCNA2 (Fig. 2f). In contrast, DAPA did not alter the phosphorylation statuses of AMPK and ACC and did not affect the expression level of CCND1 (Supplementary Fig. VII).

3.3. BM-MSCs treated with cana exhibited reduced migration and increased apoptosis

To further investigate the migration of BM-MSCs, *in vitro* Transwell migration assays were performed (Fig. 3a). The number of BM-

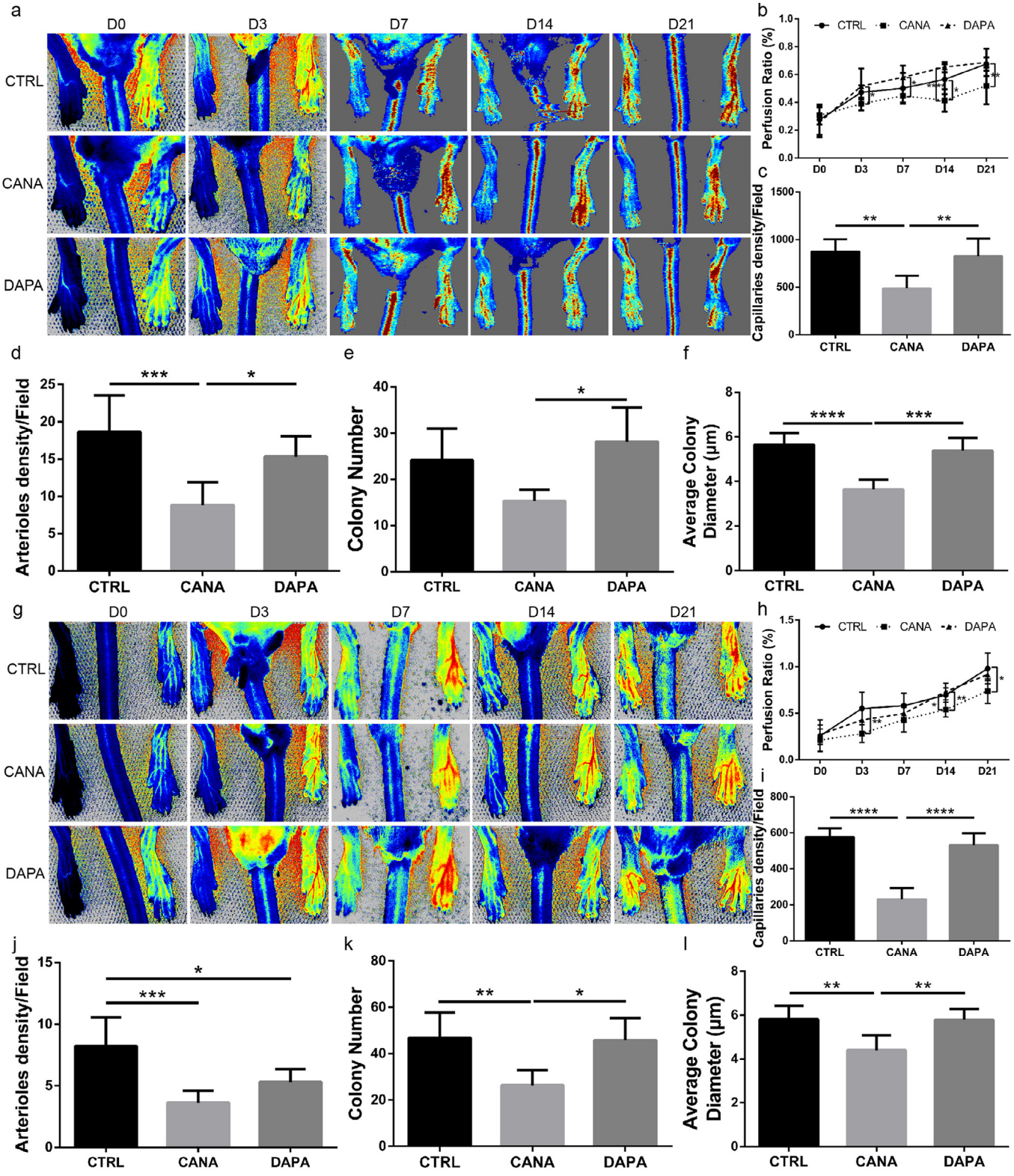

Fig. 1. CANA delayed the process of blood reperfusion and attenuated angiogenesis in the ischaemic lower limb. (a) Diabetic mice administered the CANA (10 mg/kg, $n = 6$), DAPA (1 mg/kg, $n = 6$) or vehicle control (CTRL, $n = 6$) once per day underwent femoral artery ligation (FAL) to establish ischaemia in the lower limb. Representative laser Doppler perfusion images show dynamic changes in blood perfusion of ischaemic limbs at indicated timepoints. (b) The blood flow in the lower limbs was quantitatively analysed as the ratio of the ischaemic (right) side to the nonischaemic (left) side ($n = 6$/group). Lower limb autopsy was performed 21 days after FAL in each group of mice, and immunofluorescent staining of CD31 and smooth muscle α-actin (α-SMA) was performed. (c & d) Quantification of CD31-positive endothelial cells and α-SMA-positive arterioles on the immunostained sections. BM-MSCs were obtained from the diabetic mice after the administration of CANA, DAPA or vehicle control for 28 days. (e & f) The colony numbers and diameters of each flask were obtained and quantified after 7 days of culture. (g) Normoglycemic mice (aged 8 weeks, weighing 19–22 g) administered the CANA (10 mg/kg, $n = 6$), DAPA (1 mg/kg, $n = 6$) or vehicle control (CTRL, $n = 6$) once per day underwent femoral artery ligation (FAL) to establish ischaemia in the lower limb. Representative laser Doppler perfusion images show dynamic changes in blood perfusion of ischaemic limbs at indicated timepoints. (h-l) Mice were treated as described in (g), each of the reperfusion ratio (h), capillary density (i), arteriole density (j), as well as the (k) BM-MSC colony numbers and (l) colony diameters were quantified in an approach as described in the (b-f) ($n = 6$/group). Data are presented as means ± SDs, $^{*}P < 0.05$; $^{**}P < 0.01$, $^{***}P < 0.001$, $^{****}P < 0.0001$.

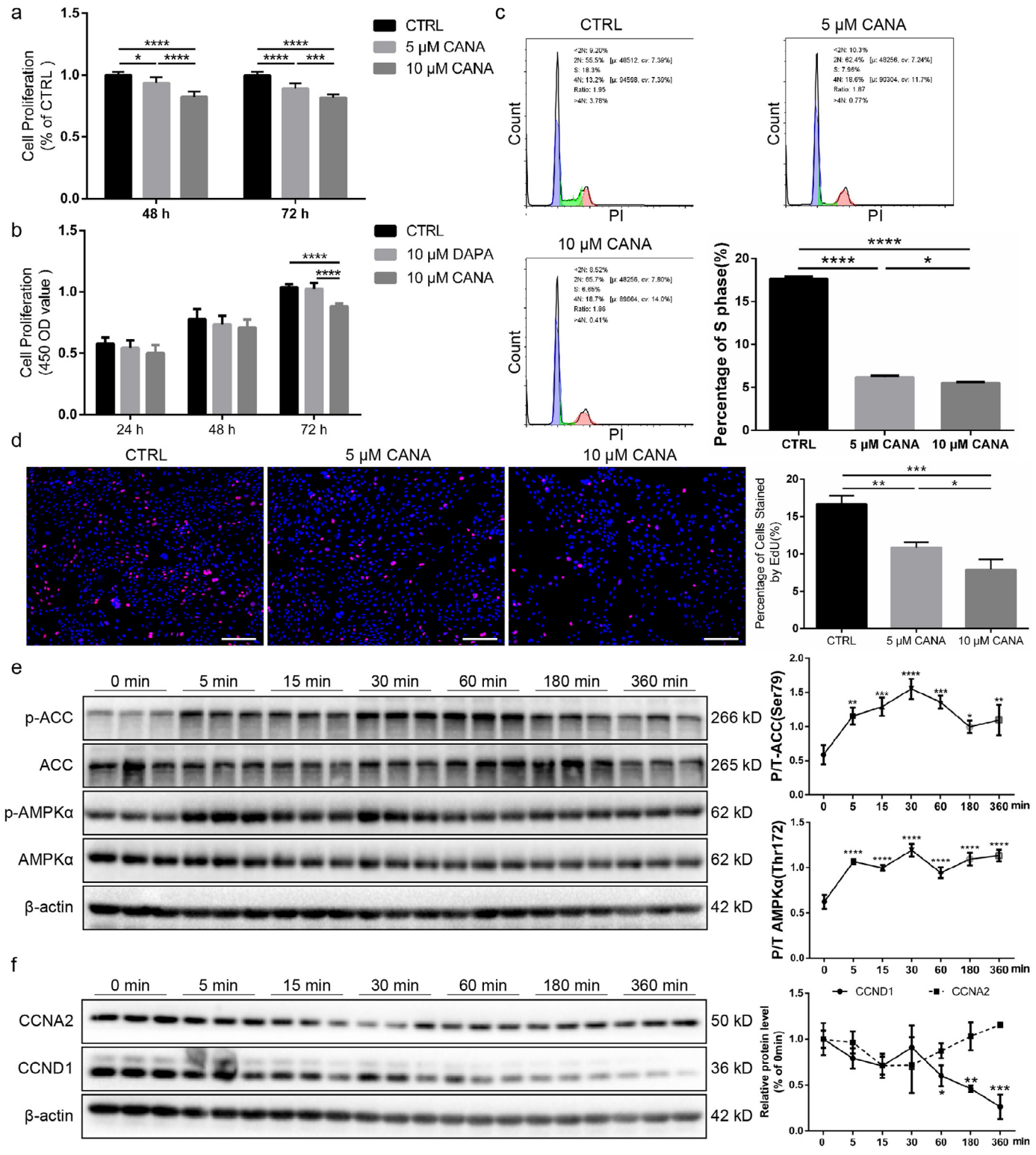

Fig. 2. CANA treatment reduced the proliferation of MSCs and downregulated CCND1 expression. (a) MSCs were incubated with CANA (5 or 10 μM) for the indicated durations, and then the medium was replaced with fresh CANA-free medium. The 0.1% DMSO-treated group served as the control (CTRL). The proliferation of MSCs was evaluated by a cell counting kit-8 (CCK-8) assay (n = 3). (b) MSCs were incubated with CANA (10 μM) and DAPA (10 μM) for the indicated durations, and the medium was then replaced with fresh CANA- and DAPA-free medium. The proliferation of MSCs in each group was detected as described in (a) (n = 3). (c) MSCs treated with CANA (5 or 10 μM, 48 h) were labelled with PI followed by cell cycle analysis by FACS. The percentage of S phase cells was calculated for each group, and the data are shown in a bar graph (n = 3). (d) MSCs were treated with CANA as described in (c) and were incubated with EdU followed by fluorescence detection by microscopy. The percentage of cells stained by EdU was calculated for each group, and the data are shown in a bar graph (n = 3), scale bar: 100 μm. (e) MSCs were treated with 10 μM CANA for 0, 5, 15, 30, 60, 180, and 360 min, and the protein expression levels of ACC, phosphorylated ACC (p-ACC), AMPKα, and phosphorylated AMPKα (p-AMPKα) were evaluated using SDS-PAGE. β-actin served as an internal reference. Quantification of protein expression is presented as the ratio of p-ACC/ACC and p-AMPKα/AMPKα, and the data are shown in a bar graph (n = 3). (f) MSCs were treated as indicated in (e), and the protein expression levels of CCNA2 and CCND1 were analysed using SDS-PAGE. Quantification of protein expression is presented as the ratio of CCNA2/β-actin and CCND1/β-actin, and the data are shown in a bar graph (n = 3). Data are means ± SDs, $^{*}P < 0.05$; $^{**}P < 0.01$, $^{***}P < 0.001$, $^{****}P < 0.0001$.

MSCs that migrated to the lower chamber was significantly decreased after treatment with 10 μM CANA compared with that obtained with the untreated and 10 μM DAPA-treated groups (Fig. 3b). Furthermore, we evaluated the migration capability of BM-MSCs using a wound healing assay. The CANA-treated groups showed inhibited migration of BM-MSCs to the scratched zone (Fig. 3c), which was quantified by indexes of wound closure and migration ratio (72 h following scratching). Wound closure was delayed by approximately 36% when the BM-MSCs were preconditioned with 10 μM CANA for 48 h and by approximately 23% when the BM-MSCs were preconditioned with 10 μM CANA for 72 h (Fig. 3d). The migration ratio was decreased by approximately 31% when the BM-MSCs were preconditioned with 10 μM CANA for 72 h (Fig. 3e). In contrast, 10 μM DAPA treatment did not attenuate the migration capability of BM-MSCs.

To determine whether CANA treatment induces apoptosis, 10 μM CANA-treated, 10 μM DAPA-treated and 0.1% DMSO (negative control) treated BM-MSCs were labelled with Annexin V and analysed by flow cytometry. Compared with the results obtained without treatment (2.2%), 10 μM CANA, but not 10 μM DAPA, increased the apoptosis rate to approximately 3.8% during culture in the presence of a low serum concentration (2% FBS) (Fig. 3f). We also evaluated the apoptosis rate of BM-MSCs during exposure to oxidative stress. Interestingly, BM-MSCs preconditioned with 10 μM CANA seemed to be more vulnerable to oxidative stress because the apoptosis rate increased to approximately 18% in the population of BM-MSCs preconditioned with 10 μM CANA compared with those found in the CTRL BM-MSCs (14%) and the population of BM-MSCs preconditioned with 10 μM DAPA (14%) (Fig. 3g). The cleaved caspase 3 expression levels determined by Western blotting were also consistent with previous findings because the cleaved caspase 3 levels increased by approximately 2-fold in the 5 μM CANA-treated BM-MSCs and 3-fold in the 10 μM CANA-treated BM-MSCs compared with those in the CTRL BM-MSCs and DAPA-treated BM-MSCs (Fig. 3h&i), which indicated that CANA-treated BM-MSCs were more vulnerable to oxidative stress.

3.4. CANA administration deteriorated cristae formation and reduced mitochondrial function

Mitochondrial function (ATP production and OCR) and integrity (tightly arranged cristae) are essential for preventing cells from undergoing apoptosis. Therefore, we hypothesized that mitochondrial dysfunction is associated with the increased apoptosis rate of BM-MSCs following CANA treatment. As expected, the ATP levels in BM-MSCs were decreased by approximately 7.8% when the BM-MSCs were preconditioned with 10 μM CANA for 48 h, whereas the ATP levels remained unchanged in the DAPA-treated BM-MSCs (Fig. 4a). Compared with untreated BM-MSCs, MSCs treated with CANA (10 μM) showed a 7% increase in mitochondrial reactive oxygen species (ROS), as evaluated using a MitoSOX staining assay (Fig. 4b), and a 22% decrease in GDH1 activity, which was evaluated using a spectrophotometric assay (Fig. 4c), but these indexes remained unchanged in BM-MSCs treated with DAPA. In addition, BM-MSCs treated with CANA (10 μM) showed a 63% decrease in the maximal OCR (under CCCP treatment) and a 29% decrease in the basal OCR (Fig. 4d) compared with untreated BM-MSCs. In contrast, decreases in the maximal and basal OCRs were not observed in BM-MSCs treated with DAPA (10 μM) (Fig. 4e). In addition to mitochondrial function, mitochondrial integrity was also assessed, and the BM-MSCs treated with CANA (10 μM), but not those treated with DAPA (10 μM), showed vacuole formation in cristae (as indicated by the black arrow in the image, Fig. 4f). Disruption of mitochondrial function and integrity, which might be the cause of the increased apoptosis rate in BM-MSCs following CANA treatment, has been shown to be associated with the release of cytochrome c and the initiation of apoptosis [19]. Indeed, cytosolic cytochrome c (Fig. 4g) and active caspase 3 (Fig. 3h) were significantly increased in the 10 μM CANA-treated BM-MSCs compared with the 10 μM DAPA and negative control treated BM-MSCs.

3.5. The paracrine function of BM-MSCs was compromised by cana treatment

It has been confirmed that BM-MSCs repair ischaemic tissue via paracrine activities, including pro-angiogenic [20] and anti-apoptotic effects [21]. Therefore, we performed *in vitro* experiments to verify whether CANA treatment attenuated the secretion of exosomes (a major component of the paracrine machinery of BM-MSCs) and VEGFA (an important cytokine secreted by BM-MSCs), which might reduce tube formation and survival of HUVECs. Compared with that found in the untreated group, the number of exosomes in the CANA-treated group decreased by approximately 36% (Fig. 5a), and the secretion of VEGFA from these BM-MSCs was decreased by approximately 15% (Fig. 5b). Culture supernatants of CANA-treated BM-MSCs (CANA MSCs) and untreated BM-MSCs (CTRL MSCs) were used to culture HUVECs (1×10^4 cells) seeded on Matrigel, and the angiogenesis ability of each group was assessed. We found that culture supernatants from untreated BM-MSCs significantly enhanced the tube formation of HUVECs. However, the medium from CANA-treated BM-MSCs caused a complete loss of this ability (Fig. 5c), which implies that CANA treatment results in attenuation of the paracrine function of BM-MSCs. Additionally, culture supernatants from untreated BM-MSCs were found to reduce H_2O_2-induced HUVEC apoptosis by 14%, while CANA treatment abrogated this protective effect (Fig. 5d).

3.6. The therapeutic efficiency of bm-msc transplantation was compromised when BM-MSCs were preconditioned with cana

To evaluate the impact of CANA on the therapeutic efficiency of BM-MSCs, we conducted an *in vivo* study aiming to assess the effects of CANA on the retention of BM-MSCs and the proangiogenic effect of BM-MSCs in ischaemic lower limb. A total of 17 8-week-old male mice, including five mice transplanted with PBS, six mice transplanted with DMSO-preconditioned BM-MSCs (control group) and six mice transplanted with CANA (10 μM, 48 h)-preconditioned BM-MSCs, were used to evaluate the retention of BM-MSCs and angiogenesis in ischaemic lower limb. To establish a more severe lower limb ischaemia model, the mice were subjected to right IAL surgery and transplanted with CANA-preconditioned BM-MSCs. Compared with the mice transplanted with DMSO-preconditioned BM-MSCs, those transplanted with CANA-preconditioned BM-MSCs had significantly lower amounts of retained BM-MSCs at days 3 and 5 (Fig. 6a&6b). Consistent with the amounts of retained BM-MSCs, the mice transplanted with CANA-preconditioned BM-MSCs exhibited reduced blood reperfusion at days 3 and 7 compared with the mice transplanted with DMSO-preconditioned BM-MSCs (Fig. 6c&6d). To evaluate the proangiogenic activity of BM-MSCs, the capillary and arteriole density in ischaemic muscles were analysed by CD31 and α-SMA immunostaining, respectively. Both the capillary (Fig. 6e) and arteriole (Fig. 6f) densities at day 21 were lower in the mice transplanted with CANA-preconditioned BM-MSCs than in the mice transplanted with DMSO-preconditioned BM-MSCs. Moreover, the extent of myofibre regeneration in the mice transplanted with CANA-preconditioned BM-MSCs was less than that in the mice transplanted with CTRL BM-MSCs, whereas the extent of myofibre regeneration in the mice transplanted with CANA-preconditioned BM-MSCs remained higher than that in mice transplanted with PBS, which indicates that myofibre regeneration might involve mechanisms other than angiogenesis (Fig. 6g&6 h).

3.7. Restoration of the secretion of vegfa by BM-MSCs reversed the therapeutic efficiency of CANA-preconditioned BM-MSCs

Our previous findings confirmed that the paracrine effects and the *in vivo* therapeutic effects of BM-MSCs were compromised by CANA treatment (Fig. 5&6). Therefore, we performed *in vivo* experiments to verify whether improving the paracrine effects of BM-MSCs could

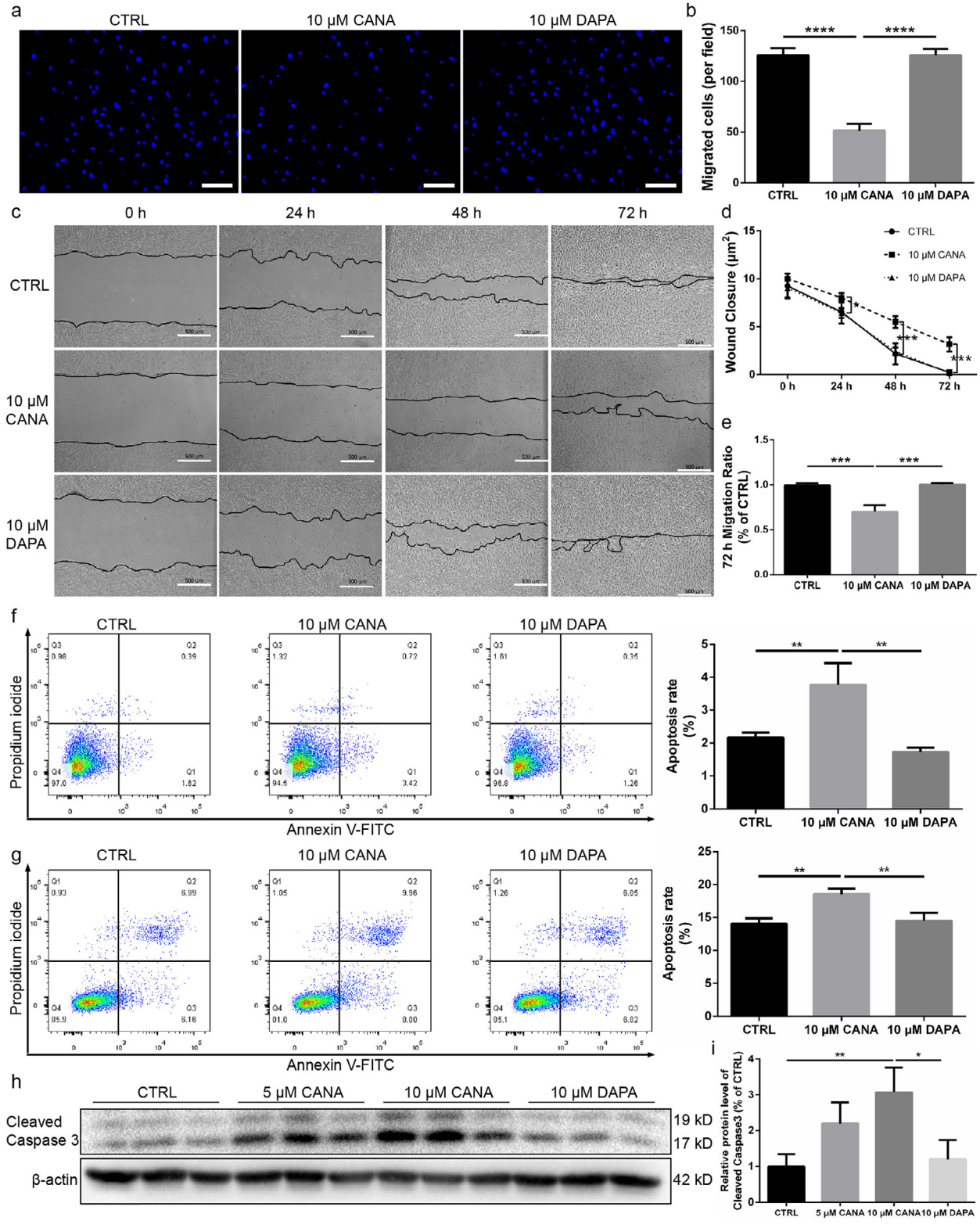

Fig. 3. CANA treatment attenuated MSC migration and increased the apoptosis of MSCs under both normal and stress conditions. (a) MSCs were treated with either CANA (10 μM) or DAPA (10 μM) for 48 h. Each group of MSCs was subjected to Transwell migration assays, and representative images of cells migrating to the lower surface are shown. Scale bars: 100 μm. (b) Cells that migrated to the lower surface were counted for each group, and the data are shown in a bar graph (n = 3). (c) MSCs were treated with either CANA or DAPA as described in (a). A wound healing assay was performed to detect the migration ability of MSCs at the indicated timepoints. Scale bars: 500 μm. (d) Wound closure of each group shown in (c) was indicated by the remaining area that was not covered by cells in the scratched zone (n = 3). (e) The migration ratio of each group (72 h following scratching) shown in (c) was quantified (n = 3). (f) CANA- (10 μM, 48 h) or DAPA-treated (10 μM, 48 h) MSCs were stained with Annexin V and PI followed by flow cytometry analysis. The apoptosis rate in each group was calculated, and the data are shown in a bar graph (n = 3). (g) CANA- (10 μM, 48 h) or DAPA-treated (10 μM, 48 h) MSCs were stimulated with or without H_2O_2 (100 nmol) for 2 h. The apoptosis rate in each group was measured and calculated as described in (f), and all the data are shown in a bar graph (n = 3). (h) MSCs were treated as mentioned in (g), and the protein expression level of cleaved caspase 3 was evaluated using SDS-PAGE. β-actin served as an internal reference. (i) Quantification of protein expression is presented as the ratio of cleaved caspase 3/β-actin, and the data are shown in a bar graph (n = 3). Data are means ± SDs, $^{*}P < 0.05$; $^{**}P < 0.01$, $^{***}P < 0.001$, $^{****}P < 0.0001$.

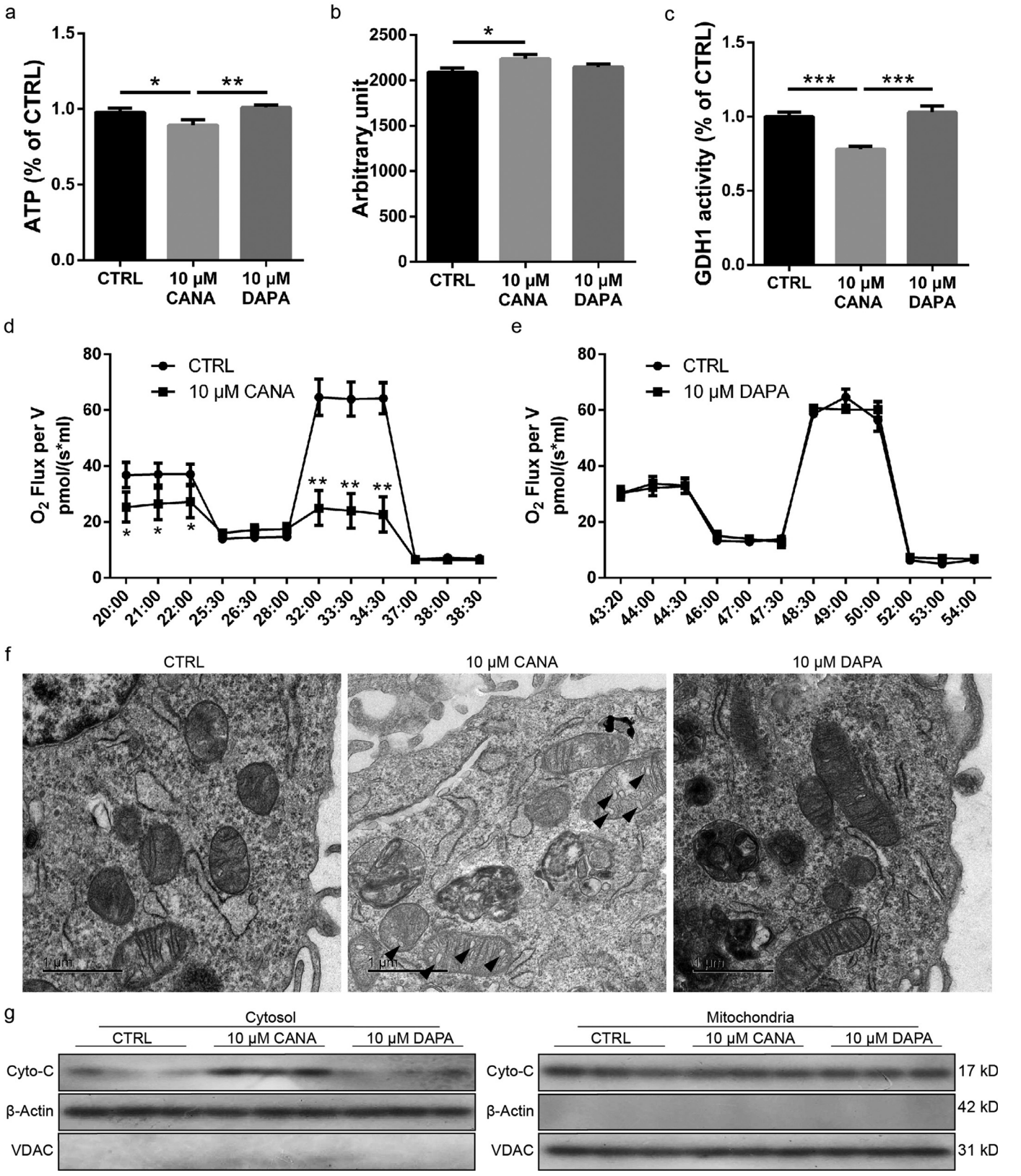

Fig. 4. CANA administration deteriorated cristae formation and reduced mitochondrial function. (a) MSCs were incubated with CANA (5 or 10 μM, 48 h) or DAPA (10 μM, 48 h). Intracellular ATP levels were determined via luciferin/luciferase-based assays (n = 3). (b) MSCs were incubated with CANA (10 μM, 48 h) or DAPA (10 μM, 48 h). Then, flow cytometry analysis was conducted to evaluate the fluorescence intensity of MitoSOX-stained MSCs (n = 3). The results are shown in a bar graph. (c) MSCs were incubated with CANA (10 μM, 48 h) or DAPA (10 μM, 48 h), and GDH1 activity was then evaluated using a spectrophotometric assay (n = 3). (d) MSCs were incubated with CANA (10 μM, 48 h). The oxygen consumption rates (OCRs) in each group of MSCs were assayed under both basal and maximal conditions (*i.e.*, under CCCP treatment; n = 3). (e) MSCs were incubated with DAPA (10 μM, 48 h). The OCR of each group was detected as described in (d) (n = 3). (f) MSCs were incubated with CANA (10 μM, 48 h) or DAPA (10 μM, 48 h). Then, the MSCs were analysed by TEM. Representative images are shown (Scale bar=1 μm). Vacuole formation in cristae is indicated by a black arrow. (g) CANA- (10 μM, 48 h) or DAPA-treated (10 μM, 48 h) MSCs were stimulated with or without H_2O_2 (100 nmol) for 2 h. Cytochrome c release was then determined by Western blot analysis of both the cytosol (left) and mitochondrial pellets (right). VDAC and β-actin served as internal references. Data are means ± SDs, $^*P < 0.05$; $^{**}P < 0.01$, $^{***}P < 0.001$.

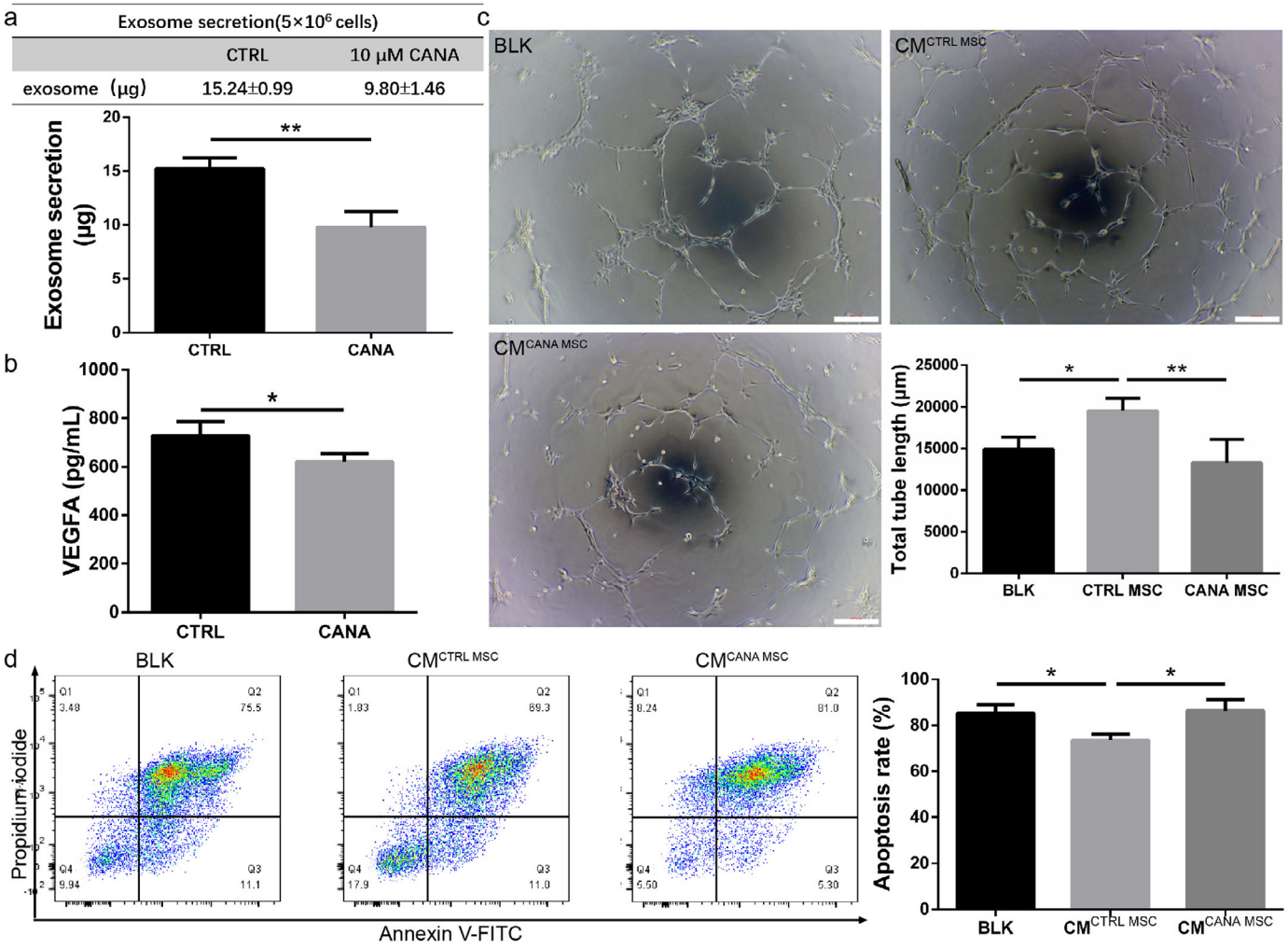

Fig. 5. The paracrine effect of MSCs was compromised by CANA treatment. (a) MSCs were treated with 10 μM CANA or 0.1% DMSO for 48 h, and then 5×10^6 cells were cultured in CANA-free DMEM supplemented with 2% exosome-free serum for an additional 24 h. Culture supernatants were collected, and exosomes were isolated using a standard ultracentrifugation method and quantified using a BCA assay. The results are presented as the amounts of exosomes secreted by 5×10^6 cells. (b) The culture supernatants from (a) were collected, and the concentration of VEGFA in the supernatant was analysed by ELISA. (c) MSCs were incubated with CANA (10 μM, 48 h), and the MSCs (4×10^5 cells) were then cultured in CANA-free M199 supplemented with 2% FBS for an additional 24 h. The supernatant of cultured MSCs in each group was collected to incubate human umbilical vein endothelial cells (HUVECs) to induce tube formation of HUVECs on Matrigel. The 0.1% DMSO-treated group served as the control (CTRL). Representative images are shown. Scale bars: 200 μm. Tube formation was quantified by measuring the total branch lengths of the formed tube ($n = 3$). (d) HUVECs were incubated in CM from the MSCs described in (a) for 24 h, and HUVECs were further conditioned by H_2O_2 (50 nmol) for 2 h to induce apoptosis. Then, the cells were stained with Annexin V and PI followed by flow cytometry analysis. The apoptosis rate in each group was calculated, and the data are shown in a bar graph ($n = 3$). Data are means ± SDs, $^*P < 0.05$; $^{**}P < 0.01$.

reverse the therapeutic efficiency of CANA-preconditioned BM-MSCs. Parental BM-MSCs were first infected with lentivirus containing mouse VEGFA to generate a stably transfected cell line ($MSCs^{VEGFA}$). Compared with $MSCs^{CTRL}$ (BM-MSCs infected with lentivirus containing empty plasmid), the VEGFA mRNA level in the $MSCs^{VEGFA}$ was increased by approximately 16-fold (Supplementary Fig. VIIIa), and VEGFA secretion was increased by 1.3-fold (Supplementary Fig. VIIIb). A total of 18 8-week-old male mice, including mice transplanted with DMSO-preconditioned $MSCs^{CTRL}$ ($MSCs^{CTRL}$, $n = 6$), CANA-preconditioned (10 μM, 48 h) $MSCs^{CTRL}$ ($MSCs^{CTRL}$+CANA, $n = 6$) and CANA-preconditioned (10 μM, 48 h) $MSCs^{VEGFA}$ ($MSCs^{VEGFA}$+CANA, $n = 6$), were used for the evaluation of angiogenesis in ischaemic lower limb. Consistent with our previous findings, blood flow recovery was delayed in the $MSCs^{CTRL}$+CANA-transplanted mice compared with the $MSCs^{CTRL}$-transplanted mice. However, blood flow recovery was markedly improved in the $MSCs^{VEGFA}$+CANA-transplanted mice (Fig. 7a&7b). At day 21, both the capillary and arteriole densities at day 21 (Fig. 7c, 7d&7e), as well as the regenerating myofibres (Fig. 7f&7 g) in ischaemic gastrocnemius muscles, were higher in the mice transplanted with $MSCs^{VEGFA}$+CANA than in those transplanted with $MSCs^{CTRL}$+CANA. Overall, the results of these *in vivo* studies imply that the attenuated angiogenesis of BM-MSCs following CANA administration might be rescued by improving the paracrine function of BM-MSCs.

3.8. CANA inhibits bm-msc GDH1 activity via binding to the ADP-binding pocket

We and Secker et al. [14] have confirmed that CANA inhibits GDH1 activity and thereby inhibits the TCA cycle and decreases ATP production. Thus, we speculate that CANA might inhibit GDH1 activity by directly interacting with GDH1 and that this interaction attenuates mitochondrial function and ATP production, leading to impairment of cellular function. To validate this hypothesis, the intermolecular interaction of CANA upon binding to GDH1 was analysed using the MOE. CANA was predicted to interact with GDH1 via hydrogen bonds with the amino acid residues Thr-A91 (A indicates the A chain in the GDH1 hexamer) (Fig. 8a). In addition, CANA formed arene interactions with the residues Pro-A125, His-B199 and Asn-B392 (Fig. 8a). Residues in the binding pocket of GDH1, including Val-

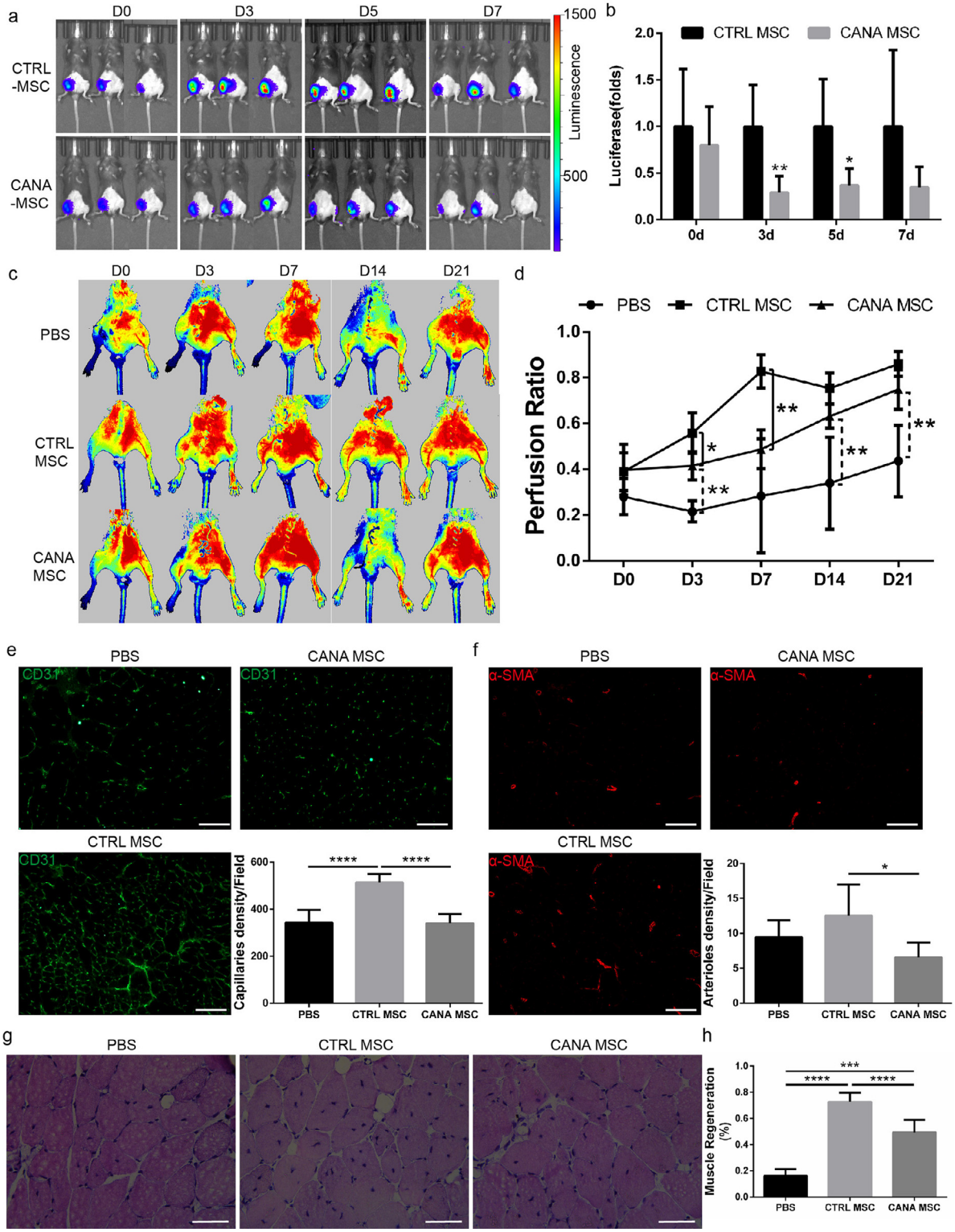

Fig. 6. The therapeutic efficiency of MSC transplantation was compromised when MSCs were preconditioned with CANA. (a) MSCs transfected with luciferase (Luc-MSCs) were incubated with 10 μM CANA for 48 h. Luc-MSCs (1×10^6 cells) were then injected into the gastrocnemius muscle at 5 points on the ischaemic (right) side ($n = 6$) 1 h after right IAL. Luc-MSCs pretreated with DMSO (0.1%) were injected into the ischaemic zone and served as a control (CTRL, $n = 6$). Representative bioluminescence images obtained with a Xenogen system at the indicated timepoints are shown, and (b) the data are presented as the fold changes in the bioluminescent intensity of CANA *vs.* CTRL at the indicated timepoints. (c) Mice were treated as described in (a), and representative laser Doppler perfusion images show the extent of blood perfusion recovery in ischaemic limbs at the indicated timepoints. (d) The blood flow in the lower limbs was quantitatively analysed as the ratio of the blood flow in the ischaemic (right) side to that in the nonischaemic (left) side. The data are shown in a bar graph ($n = 5$ or 6/group). (e) Mice were treated as described in (a), lower limb gastrocnemius muscle autopsy was performed 21 days after IAL in each group of mice, and immunofluorescent staining of CD31 was performed. Representative images and the quantification of CD31-positive endothelial cells are shown (scale bar: 100 μm). (f) Immunofluorescence staining of smooth muscle α-actin (α-SMA) of mice described in (e), and representative images and the quantification of α-SMA-positive arterioles are shown (scale bar: 100 μm). (g) Mice were treated as described in (a), and representative haematoxylin and eosin-stained sections of ischaemic muscles from each group at day 21 are shown (scale bar: 50 μm); myocytes with centralized nuclei were considered regenerating myofibres. (h) Regenerating myofibres shown in (g) were quantified by counting myocytes with centralized nuclei as a percentage of total myocytes in a field of view. Data are means ± SDs, $^*P < 0.05$; $^{**}P < 0.01$, $^{***}P < 0.001$, $^{****}P < 0.0001$.

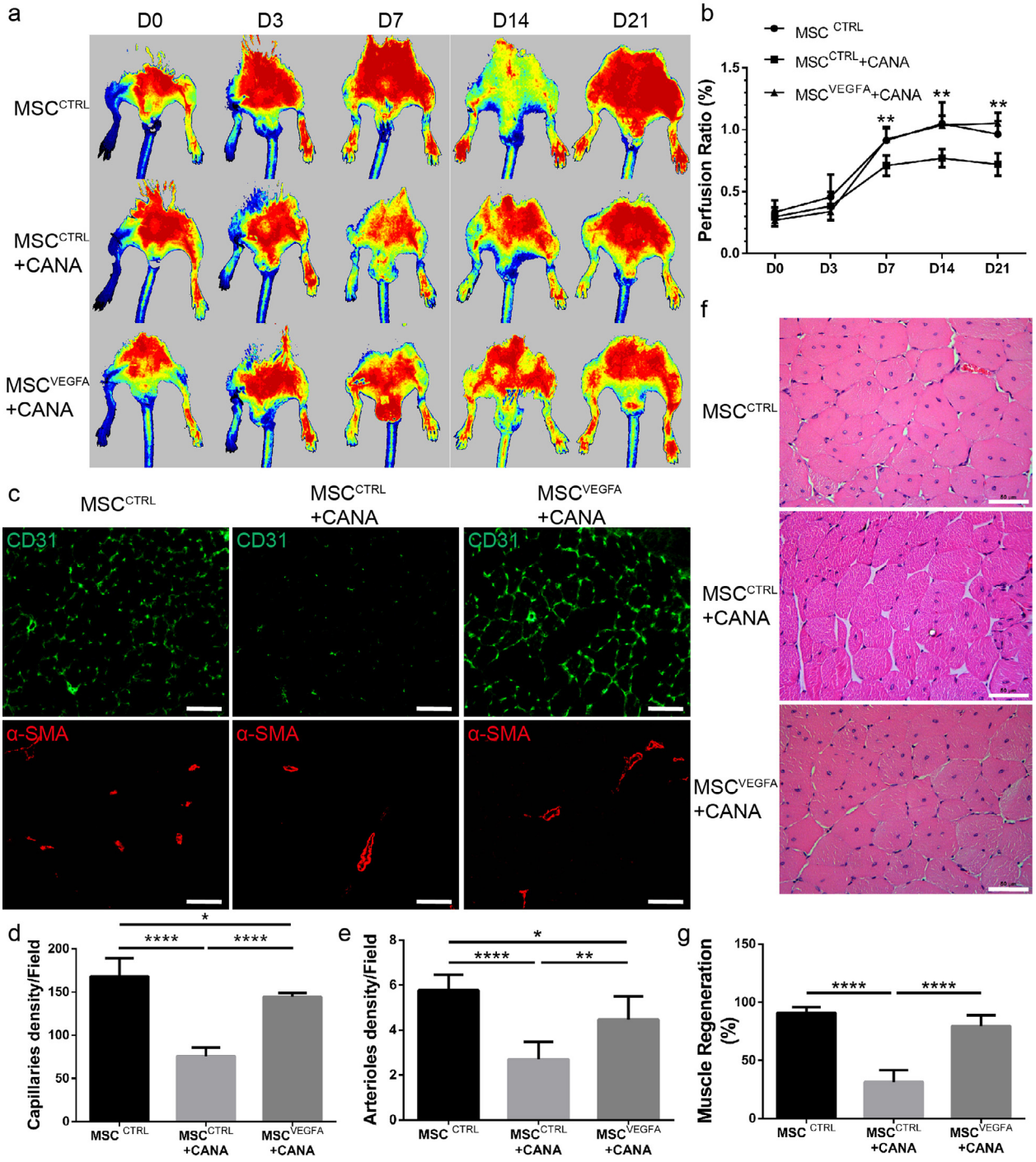

Fig. 7. VEGFA overexpression rescued the therapeutic efficiency of CANA-preconditioned MSCs. VEGFA-overexpressing MSCs ($MSCs^{VEGFA}$) or control lentivirus-infected MSCs ($MSCs^{CTRL}$) were incubated with 10 μM CANA for 48 h. The cells (1×10^6 cells) were then injected into the gastrocnemius muscle at five points on the ischaemic (right) side ($n = 6$) 1 h after right FAL. $MSCs^{CTRL}$ pretreated with DMSO (0.1%) were injected into the ischaemic zone and served as a control (CTRL, $n = 6$). The extent of blood perfusion recovery in the ischaemic limbs at the indicated timepoints was measured by laser Doppler, and representative images are shown. (b) The blood flow in the lower limbs was quantitatively analysed as the ratio of the blood flow in the ischaemic (right) side to the that in the nonischaemic (left) side. The data are shown in a bar graph ($n = 6$/group). (c) Mice were treated as described in (a), lower limb gastrocnemius muscle autopsy was performed 21 days after FAL, and immunofluorescent staining of CD31 and α-SMA was also performed. Representative images are shown (Scale bar: 200 μm). (d) Quantification of CD31-positive endothelial cells on the immunostained sections shown in (c) ($n = 6$/group). (e) Quantification of α-SMA-positive arterioles in (c) ($n = 6$/group). (f) Representative haematoxylin-and-eosin-stained sections of ischaemic muscles from each group at day 21 (scale bar: 50 μm). (g) Quantification of regenerating myofibres in (f); the data are shown as the percentages of myocytes with centralized nuclei within the total number of myocytes in a field of view ($n = 6$/group). Data are means ± SDs, $^*P < 0.05$; $^{**}P < 0.01$; $^{****}P < 0.0001$.

A124, Ala-B198, Val-B396 and Ala-A120, form hydrophobic interactions with atoms in CANA. The spatial interactions between CANA and residues in GDH1 were also analysed in a 3D model (Fig. 8b). The sidechains of Thr-A91 served as hydrogen bond donors. ADP is a potent activator of GDH1. The literature has described the detailed docking mode of ADP upon interaction with GHD1 [22]. By analysing the binding pocket (formed by Pro-A125, Arg-A90, Asp-A123, Lys-B391, Ser-B397 and Arg-B400) in GDH1 complexed with CANA (Fig. 8a), we found that ADP and CANA share the same binding pocket in GDH1. The 3D structure of the CANA-GDH1 complex is shown in

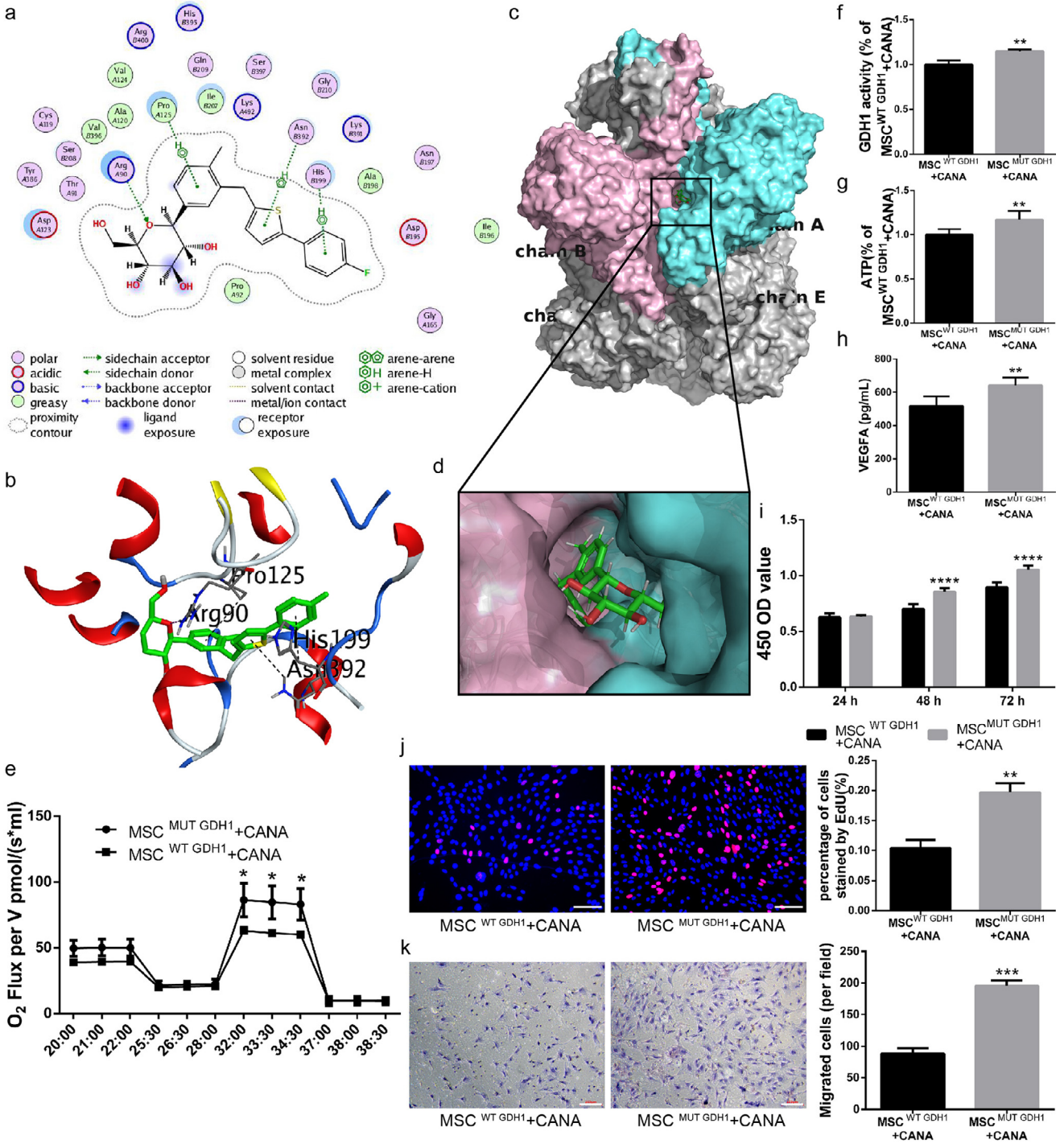

Fig. 8. CANA interacts with the GDH1 hexamer by binding to a pocket formed by Chains A and B. (a) Docking simulations between CANA and GDH1 were performed using MOE software, which provided a 2D diagram of CANA/GDH1. The chemical structure of CANA is shown in the center, and its key interacting amino acids are shown around the structure. The annotations for the atom properties and interaction patterns were shown below. A and B in the circle of residue names denote Chains A and B of the GHD1 hexamer. The proximity contour indicates the amount of space that is available for substitutions on the ligand. Ligand exposure: the smudges drawn behind some of the ligand atoms indicate the solvent-accessible surface area of the ligand; receptor exposure: the size and intensity of the blue circle behind the residues correlated with the extent of solvent exposure of the corresponding residues as a result of the present of the ligand. (b) A 3D model of the docking poses of CANA with the GDH1 hexamer is shown. The purple dotted lines indicate hydrogen bonds; the green dotted lines indicate arene interactions; and the distance (expressed in Å) between atoms is provided for each hydrogen bond and arene interaction. Oxygen atoms are marked in red; nitrogen atoms are marked in blue; and sulfur atoms are marked in yellow. (c) CANA docks into the binging pocket of the GDH1 hexamer formed by Chains A (whose surface is shown in aquamarine) and B (whose surface is shown in pink); the surface of the other chains of the GHD1 hexamer are shown in gray. (d) A magnified view of the docking interface is displayed on the lower panel. (e) MSCs were first transfected with shRNA targeting mouse GDH1. These cells were then infected with recombinant lentiviruses carrying wild-type (WT) or H199A and N392A mutant (MUT) GDH1 cDNA ($MSCs^{WT\ GDH1}$ or $MSCs^{MUT\ GDH1}$). The resulting $MSCs^{WT\ GDH1}$ and $MSCs^{MUT\ GDH1}$ were incubated with CANA (10 μM, 48 h), and their OCRs were assayed under both basal and maximal conditions (*i.e.*, under CCCP treatment; $n = 3$). (f) $MSCs^{WT\ GDH1}$ and $MSCs^{MUT\ GDH1}$ were incubated with CANA (10 μM, 48 h), their GDH1 activity was evaluated using a spectrophotometric assay ($n = 3$), and (g) their intracellular ATP levels were determined via luciferin/luciferase-based assays. (h) The cells were treated as indicated in (f), and 5×10^6 cells were cultured in CANA-free DMEM supplemented with 2% FBS for an additional 24 h. The culture supernatants were collected, and the concentration of VEGFA in the supernatant was analysed by ELISA. (i) The cells were treated as indicated in (f), and the proliferation of MSCs was evaluated by a CCK-8 assay ($n = 3$) and (j) an EdU staining assay (Scale bar: 100 μm). (k) The migration ability of the cells was evaluated using a Transwell migration assay (Scale bar: 100 μm). Data are means ± SDs, $^*P < 0.05$; $^{**}P < 0.01$, $^{***}P < 0.001$, $^{****}P < 0.0001$.

Fig. 8c, and the corresponding binding pocket is magnified in Fig. 8d. This analysis indicates that CANA docks into a binding pocket of the GDH1 hexamer formed by Chains A and B. Based on the docking simulation conducted in the MOE, we infer that CANA might competitively binds to the binding pocket in the hexamer of GDH1, which abrogates the role of ADP in GDH1 activation.

We then generated BM-MSCs expressing wild-type GDH1 ($MSC^{WT\ GDH1}$) or H199A and N392A mutant GDH1 ($MSC^{MUT\ GDH1}$). The expression of GDH1 in $MSCs^{WT\ GDH1}$ and $MSCs^{MUT\ GDH1}$ and the GDH1 activities in $MSCs^{WT\ GDH1}$ and $MSCs^{MUT\ GDH1}$ were comparable (Supplementary Fig. IXa&b). Interestingly, $MSCs^{MUT\ GDH1}$ treated with CANA (10 μM, 48 h) showed a 37% increase in the maximal OCR (under CCCP treatment) and a 27% increase in the basal OCR compared with CANA-treated $MSCs^{WT\ GDH1}$ (Fig. 8e). GDH1 activity (Fig. 8f), ATP production (Fig. 8g) and VEGFA secretion (Fig. 8h) in CANA-treated $MSCs^{MUT\ GDH1}$ were elevated by 15%, 17% and 24% compared with the those obtained with CANA-treated $MSC^{WT\ GDH1}$, respectively. In addition, the proliferation of CANA-treated $MSCs^{MUT\ GDH1}$ evaluated by the CCK-8 and EdU staining assays (Fig. 8i&8j) and their migration ability evaluated using a Transwell assay (Fig. 8k) were also increased compared with those of CANA-treated $MSCs^{WT\ GDH1}$. Taken together, the aforementioned data imply that CANA docks into the binding pocket of the GDH1 hexamer to competitively inhibit the interaction between ADP and GDH1-hexamer and thereby attenuate the catalytic activity of GDH1 in BM-MSCs.

3.9. Discussion

Recent clinical findings have indicated that CANA treatment is associated with an increase in amputation risk [7]. Our investigation also revealed that the treatment of diabetic and nondiabetic mice with CANA for 21 days impairs angiogenesis and muscle regeneration in ischaemic skeletal muscle, which in turn delays the recovery of ischaemic lower limbs. A subsequent investigation seeking the possible mechanism responsible for the aforementioned phenomenon led us to the possibility that the biological functions of BM-MSCs are impaired by CANA. This hypothesis was confirmed by the following evidence: (1) the proliferation capacity and migration ability of BM-MSCs were compromised by CANA treatment; (2) the number of exosomes in CANA-treated BM-MSCs and their secretion of VEGFA, which is as an important parameter of BM-MSC paracrine function, were also reduced; (3) the proangiogenic and prosurvival effects of BM-MSCs were both abrogated by CANA; and (4) CANA increased the apoptosis of BM-MSCs during culture in the presence of a low serum concentration (2%) and under oxidative stress conditions. These *in vitro* findings might be explained by impaired mitochondrial function, which was demonstrated by reductions in ATP production, cellular OCR, and GDH1 activity. Furthermore, the *in vivo* results were also consistent with our previous findings that CANA attenuated the protective effects of BM-MSCs, as demonstrated by the finding that the injection of CANA-pretreated BM-MSCs into ischaemic muscles resulted in impairments in blood flow recovery, angiogenesis and muscle regeneration in the ischaemic limbs.

MSCs reside in several adult tissues [23]. Endogenous BM-MSCs can be mobilized to the peripheral blood under hypoxic stimulation [24] or due to organ/tissue damage [25,26], migrate to sites of injury in response to chemoattractive factors and endogenous electric fields at wounds, and participate in the repair process [27]. BM-MSCs have been proven to accelerate and improve muscle function recovery after muscle injury [28]. However, the exposure of MSCs to toxic conditions, such as cigarette smoking or hyperglycaemia, impairs their biological functions [29,30], and MSCs are ineffective at improving tissue ischaemia [31]. The present study revealed that CANA administration attenuated the colony formation capability of endogenous BM-MSCs. Our results also indicated the possible effects of impaired BM-MSC functions in the aforementioned clinical findings, which unveiled the fact that the biological functions of BM-MSCs, including proliferation, migration and paracrine function, are all attenuated by CANA.

Gliflozins (CANA, DAPA and empagliflozin) are inhibitors of members of SGLTs and primarily target SGLT2, which is expressed in renal proximal tubule epithelial cells (RPTECs) of the kidney [32] and is responsible for the bulk of renal glucose reabsorption. Recently, SGLT2 has also been reported to be expressed in certain cancer cells (pancreatic and prostate adenocarcinomas) [33], and SGLT2 functions as an important glucose transporter in these cells. Our data suggest that BM-MSCs express SGLT2 at a relatively low level (Supplementary Fig. X). However, there is no direct evidence that CANA modulates cellular metabolism via SLGT2 inhibition. Our current study also confirmed that only CANA treatment, instead of DAPA treatment, decreases cellular ATP production and dramatically impairs the OCR of BM-MSCs, implying that SGLT2 is not involved in the adverse effect of CANA on BM-MSCs. Several studies have reported that CANA simultaneously inhibits glutamate dehydrogenase (GDH) and mitochondrial electron transport chain (ETC) complex I at clinically relevant concentrations [14,34], which suggests the possibility that the function and/or architecture of mitochondria are the targets of CANA.

Recently, CANA has been reported to accelerate blood perfusion recovery in severe limb ischaemia induced by FAL in nonobese diabetic/severe combined immunodeficient (NOD/SCID) mice [35]. However, our findings indicated that CANA hindered the perfusion recovery in diabetic C57BL/6 mice at days 14 and 21 despite the decrease in the blood glucose level. This may due to the blood glucose levels of CANA and DAPA administered mice remained relatively higher than normal mice, which attenuated the biological function of BM-MSCs per se. This discrepancy also indicated that the inflammatory response, which is also affected by CANA [36], plays important roles in angiogenesis and blood flow recovery in an ischaemic limb. To exclude the toxic effect of hyperglycaemia on BM-MSCs, nondiabetic C57BL/6 mice were also used for establishment of the lower limb ischaemia animal model. This model might indicate the net effects of CANA on angiogenesis and blood flow recovery *in vivo*, and the results also indicated that CANA hindered the perfusion recovery in normoglycemic mice. According to previous clinical findings, amputation risk increases among patients with prior amputation and preexisting peripheral artery disease [7]. Although lower limb ischaemia induced by FAL or IAL cannot be used to evaluate chronic limb ischaemia as a result of progressive atherosclerosis, it is a commonly accepted model for the induction of acute and severe limb ischaemia, which partially mimic the clinical pathological progression of peripheral artery diseases [37].

BM-MSCs require adequate energy and substrates to synthesize cytokines and modulation factors. The paracrine function of BM-MSCs, namely, the synthesis of cytokines and modulation factors, as well as the formation and secretion of vesicles, are all ATP-consuming processes [38]. Several studies have emphasized that successful transition through the cell cycle requires the integration of phases of the cell cycle with adaptive changes in both metabolism and the mitochondrial network [39,40]. Therefore, mitochondrial homeostasis and adequate ATP supply are greatly important to the fluency of these processes. We discovered that CANA impairs the function of BM-MSC mitochondria, reduces cellular ATP production, and in turn attenuates the proliferation capability and paracrine function of BM-MSCs. AMPK is an energy sensor involved in regulating energy balance at both the cellular and whole-body levels [41]. AMPK is activated due to inhibition of complex I of the respiratory chain by CANA [34], as was confirmed in our study because CANA increased AMPK Thr172 phosphorylation. In addition, AMPK activation is associated with G1 arrest [42] and is accompanied by degradation of CCND1 [43], both of which were observed in our study. The activation of AMPK by CANA also increased the phosphorylation of ACC at Ser79, which is a site that is regulated by AMPK to inhibit lipid synthesis [18,44]. BM-MSCs are

challenged by a severe microenvironment and tend to undergo apoptosis when they migrate into ischaemic tissues [45]. The mitochondrial pathway is one of the important regulatory pathways of apoptosis [46]. Our findings indicated that CANA increases the release of cytochrome c in BM-MSCs under stress conditions and thus increases the apoptosis of BM-MSCs. The *in vivo* study of Luc-MSC retention also confirmed that BM-MSCs preconditioned with CANA are more vulnerable to rigorous conditions in ischaemic tissue.

Mammalian GDH1 is activated when complexed with ADP. ADP activates GDH1 by facilitating the opening of the catalytic cleft [47]. Based on our analysis of the crystal structure of GDH1 complexed with ADP and the docking simulation between GDH1 and CANA, we found that ADP and CANA share the same binging pocket in the GDH1 hexamer. In addition, ADP forms a main chain contact with Pro125 in GDH1 [22], and CANA formed a hydrogen bond with Pro-A125 in our simulation. Thus, we infer that CANA docks into the binding pocket of the GDH1 hexamer to competitively inhibit the interaction between ADP and the GDH1 hexamer, leading to attenuation of the catalytic activity of GDH1 in BM-MSCs. Because the sidechains of His-B199 and Asn-B392 in the GDH1 hexamer form arene interactions with CANA, we constructed a mutant, H199A-GDH1/N392A-GDH1 (the His-residue in position 199 and the Asn-residue in position 392 in GHD1 were mutated to Ala), to abrogate the binding between GDH1 and CANA. As expected, the inhibitory effects of CANA on GDH1 activity were partially abrogated in BM-MSCs expressing the H199A-GDH1/N392A-GDH1 mutant; specifically, ATP production and various capabilities of BM-MSCs, such as proliferation and migration, were also abrogated.

In this study, we found that CANA treatment attenuated blood flow recovery in severe lower limb ischaemia in nondiabetic mice, which might be due to impairments in the proliferation, migration capability, and paracrine function of BM-MSCs and reduced retention of BM-MSCs in ischaemic muscle. These effects of CANA are mediated by inhibition of the TCA cycle through the direct interaction of CANA with hexamer of GDH1 and the subsequent inhibition of GDH1 enzymatic activity, which reduces the production of ATP and disrupts mitochondrial homeostasis. These findings suggest an off-target adverse effect of CANA on blood flow recovery in ischaemic tissue independent of SGLT2 inhibition, which may provide a novel explanation for the CANA-induced increase in amputation risk in patients with prior amputations and/or the presence of peripheral artery disease and suggests that a refined therapeutic strategy for CANA is urgently required for these patients.

Declaration of Competing Interest

All of the authors declare no conflicts of interest.

Acknowledgements

We thank Beibei Wang in the Center of Cryo-Electron Microscopy (CCEM), Zhejiang University for her technical assistance on Transmission Electron Microscopy.

Funding sources

This study was financially supported by the National Natural Science Foundation of China (grant # 81800314 to J. N.), the Natural Science Foundation of Zhejiang Province (grant # LQ18H090007 to Z. L.) and the Wenzhou Science and Technology Bureau Foundation (grant #Y20190163 to Y. L.). The funding sources had no involvement in the study design, data collection, data analysis, interpretation, or writing of the report.

Author contributions

Y.N.L. and J.L.N. conceived and designed the study, performed the data analysis and interpretation and wrote the manuscript. X.H.L and C.Z. performed the *in vivo* experiments. J.S performed the *in vitro* experiments. X.C. provided study materials. X.M.L. performed histological analysis. P. X. collected and assembled the data. Z.T.W. and Z.Z.L. provided overall supervision of the project, final approval of manuscript and financial support.

Supplementary materials

Supplementary material associated with this article can be found in the online version at doi:10.1016/j.ebiom.2020.102637.

References

[1] Sun YN, Zhou Y, Chen X, Che WS, Leung SW. The efficacy of dapagliflozin combined with hypoglycaemic drugs in treating type 2 diabetes mellitus: meta-analysis of randomised controlled trials. BMJ Open 2014;4(4):e004619.
[2] Liakos A, Karagiannis T, Athanasiadou E, Sarigianni M, Mainou M, Papatheodorou K, et al. Efficacy and safety of empagliflozin for type 2 diabetes: a systematic review and meta-analysis. Diabetes Obes Metab 2014;16(10):984–93.
[3] Yang XP, Lai D, Zhong XY, Shen HP, Huang YL. Efficacy and safety of canagliflozin in subjects with type 2 diabetes: systematic review and meta-analysis. Eur J Clin Pharmacol 2014;70(10):1149–58.
[4] Verma S, Mazer CD, Al-Omran M, Inzucchi SE, Fitchett D, Hehnke U, et al. Cardiovascular outcomes and safety of empagliflozin in patients with type 2 diabetes mellitus and peripheral artery disease: a subanalysis of EMPA-REG OUTCOME. Circulation 2018;137(4):405–7.
[5] Birkeland KI, Jorgensen ME, Carstensen B, Persson F, Gulseth HL, Thuresson M, et al. Cardiovascular mortality and morbidity in patients with type 2 diabetes following initiation of sodium-glucose co-transporter-2 inhibitors *versus* other glucose-lowering drugs (CVD-REAL Nordic): a multinational observational analysis. Lancet Diabet Endocrinol 2017;5(9):709–17.
[6] Doggrell SA. Cardiovascular outcomes with canagliflozin - is it on the CANVAS? Expert Opin Pharmacother 2018;19(2):163–6.
[7] Neal B, Perkovic V, Mahaffey KW, de Zeeuw D, Fulcher G, Erondu N, et al. Canagliflozin and cardiovascular and renal events in type 2 diabetes. N England J Med 2017;377(7):644–57.
[8] Fadini GP, Avogaro A. SGLT2 inhibitors and amputations in the US FDA adverse event reporting system. Lancet Diabet Endocrinol 2017;5(9):680–1.
[9] Rochefort GY, Delorme B, Lopez A, Herault O, Bonnet P, Charbord P, et al. Multipotential mesenchymal stem cells are mobilized into peripheral blood by hypoxia. Stem Cells 2006;24(10):2202–8.
[10] M O, S Y, N A, Y I, T Y, K T. Mobilization of bone marrow-derived mesenchymal stem cells into the injured tissues after intraarticular injection and their contribution to tissue regeneration. %A Agung M. Knee Surg Sport Traumatol Arthrosc 2006;14(12):1307–14.
[11] Barbash IM, Chouraqui P, Baron J, Feinberg MS, Etzion S, Tessone A, et al. Systemic delivery of bone marrow-derived mesenchymal stem cells to the infarcted myocardium: feasibility, cell migration, and body distribution. Circulation 2003;108(7):863–8.
[12] De Bari C, Dell'Accio F, Vandenabeele F, Vermeesch JR, Raymackers JM, Luyten FP. Skeletal muscle repair by adult human mesenchymal stem cells from synovial membrane. J. Cell Biol. 2003;160(6):909–18.
[13] Fujita R, Tamai K, Aikawa E, Nimura K, Ishino S, Kikuchi Y, et al. Endogenous mesenchymal stromal cells in bone marrow are required to preserve muscle function in mdx mice. Stem Cells 2015;33(3):962–75.
[14] Secker P, Beneke S, Schlichenmaier N, Delp J, Gutbier S, Leist M, et al. Canagliflozin mediated dual inhibition of mitochondrial glutamate dehydrogenase and complex I: an off-target adverse effect. Cell Death Dis 2018;9(2):226.
[15] Shou K, Niu Y, Zheng X, Ma Z, Jian C, Qi B, et al. Enhancement of bone-marrow-derived mesenchymal stem cell angiogenic capacity by npwt for a combinatorial therapy to promote wound healing with large defect. Biomed Res Int 2017;2017:7920265.
[16] Oskowitz A, McFerrin H, Gutschow M, Carter ML, Pochampally R. Serum-deprived human multipotent mesenchymal stromal cells (MSCs) are highly angiogenic. Stem Cell Res 2011;6(3):215–25.
[17] Ferrari G, Cusella-De Angelis G, Coletta M, Paolucci E, Stornaiuolo A, Cossu G, et al. Muscle regeneration by bone marrow-derived myogenic progenitors. Science 1998;279(5356):1528–30.
[18] Villani LA, Smith BK, Marcinko K, Ford RJ, Broadfield LA, Green AE, et al. The diabetes medication Canagliflozin reduces cancer cell proliferation by inhibiting mitochondrial complex-I supported respiration. Mol Metab 2016;5(10):1048–56.
[19] Ow YP, Green DR, Hao Z, Mak TW. Cytochrome c: functions beyond respiration. Nat Rev Mol Cell Biol 2008;9(7):532–42.
[20] Spees JL, Lee RH, Gregory CA. Mechanisms of mesenchymal stem/stromal cell function. Stem Cell Res Ther 2016;7(1):125.

[21] Khubutiya MS, Vagabov AV, Temnov AA, Sklifas AN. Paracrine mechanisms of proliferative, anti-apoptotic and anti-inflammatory effects of mesenchymal stromal cells in models of acute organ injury. Cytotherapy 2014;16(5):579–85.
[22] S B, T S, J F, CA S, TJ S. Structural studies on ADP activation of mammalian glutamate dehydrogenase and the evolution of regulation. Biochemistry 2003;42(12):3446–56.
[23] Conget PA, Minguell JJ. Phenotypical and functional properties of human bone marrow mesenchymal progenitor cells. J Cell Physiol 1999;181(1):67–73.
[24] Liu L, Yu Q, Fu S, Wang B, Hu K, Wang L, et al. CXCR4 antagonist AMD3100 promotes mesenchymal stem cell mobilization in rats preconditioned with the hypoxia-mimicking agent cobalt chloride. Stem Cells Dev 2018;27(7):466–78.
[25] Mansilla E, Marin GH, Drago H, Sturla F, Salas E, Gardiner C, et al. Bloodstream cells phenotypically identical to human mesenchymal bone marrow stem cells circulate in large amounts under the influence of acute large skin damage: new evidence for their use in regenerative medicine. Transplant Proc 2006;38(3):967–9.
[26] Ramirez M, Lucia A, Gomez-Gallego F, Esteve-Lanao J, Perez-Martinez A, Foster C, et al. Mobilisation of mesenchymal cells into blood in response to skeletal muscle injury. Br J Sports Med 2006;40(8):719–22.
[27] Li L, Jiang J. Regulatory factors of mesenchymal stem cell migration into injured tissues and their signal transduction mechanisms. Front Med 2011;5(1):33–9.
[28] Andrade BM, Baldanza MR, Ribeiro KC, Porto A, Pecanha R, Fortes FS, et al. Bone marrow mesenchymal cells improve muscle function in a skeletal muscle re-injury model. PLoS One 2015;10(6):e0127561.
[29] Greenberg JM, Carballosa CM, Cheung HS. Concise review: the deleterious effects of cigarette smoking and nicotine usage and mesenchymal stem cell function and implications for cell-based therapies. Stem Cells Transl Med 2017;6(9):1815–21.
[30] Tan J, Zhou L, Zhou Y, Xue P, Wu G, Dong G, et al. The influence of diabetes mellitus on proliferation and osteoblastic differentiation of MSCs. Curr Stem Cell Res Ther 2017;12(5):388–400.
[31] Kim H, Han JW, Lee JY, Choi YJ, Sohn YD, Song M, et al. Diabetic mesenchymal stem cells are ineffective for improving limb ischemia due to their impaired angiogenic capability. Cell Transp 2015;24(8):1571–84.
[32] Chao EC, Henry RR. SGLT2 inhibition–a novel strategy for diabetes treatment. Nat Rev Drug Discov 2010;9(7):551–9.
[33] Scafoglio C, Hirayama BA, Kepe V, Liu J, Ghezzi C, Satyamurthy N, et al. Functional expression of sodium-glucose transporters in cancer. Proc Natl Acad Sci U S A 2015;112(30):E4111–9.
[34] Hawley SA, Ford RJ, Smith BK, Gowans GJ, Mancini SJ, Pitt RD, et al. The Na+/Glucose cotransporter inhibitor canagliflozin activates AMPK by inhibiting mitochondrial function and increasing cellular amp levels. Diabetes 2016;65(9):2784–94.
[35] Sherman SE, Bell GI, Teoh H, Al-Omran M, Connelly KA, Bhatt DL, et al. Canagliflozin improves the recovery of blood flow in an experimental model of severe limb ischemia. JACC 2018;3(2):327–9.
[36] Xu C, Wang W, Zhong J, Lei F, Xu N, Zhang Y, et al. Canagliflozin exerts anti-inflammatory effects by inhibiting intracellular glucose metabolism and promoting autophagy in immune cells. Biochem Pharmacol 2018;152:45–59.
[37] Putman DM, Liu KY, Broughton HC, Bell GI, Hess DA. Umbilical cord blood-derived aldehyde dehydrogenase-expressing progenitor cells promote recovery from acute ischemic injury. Stem Cells 2012;30(10):2248–60.
[38] Reeds PJ, Wahle KW, Haggarty P. Energy costs of protein and fatty acid synthesis. Proc Nutr Soc 1982;41(2):155–9.
[39] Mitra K, Wunder C, Roysam B, Lin G, Lippincott-Schwartz J. A hyperfused mitochondrial state achieved at G1-S regulates cyclin E buildup and entry into S phase. Proc Natl Acad Sci U S A 2009;106(29):11960–5.
[40] Montemurro C, Vadrevu S, Gurlo T, Butler AE, Vongbunyong KE, Petcherski A, et al. Cell cycle-related metabolism and mitochondrial dynamics in a replication-competent pancreatic beta-cell line. Cell Cycle 2017;16(21):2086–99.
[41] Hardie DG. AMPK–sensing energy while talking to other signaling pathways. Cell Metab 2014;20(6):939–52.
[42] Cai X, Hu X, Tan X, Cheng W, Wang Q, Chen X, et al. Metformin induced ampk activation, G0/G1 phase cell cycle arrest and the inhibition of growth of esophageal squamous cell carcinomas in vitro and in vivo. PLoS ONE 2015;10(7):e0133349.
[43] H G, Y K, H A, DN D, YS S. Metformin induces degradation of cyclin D1 via AMPK/GSK3β axis in ovarian cancer. Mol Carcinog 2017;56(2):349–58.
[44] Fullerton MD, Galic S, Marcinko K, Sikkema S, Pulinilkunnil T, Chen ZP, et al. Single phosphorylation sites in Acc1 and Acc2 regulate lipid homeostasis and the insulin-sensitizing effects of metformin. Nat Med 2013;19(12):1649–54.
[45] Zeng L, Hu Q, Wang X, Mansoor A, Lee J, Feygin J, et al. Bioenergetic and functional consequences of bone marrow-derived multipotent progenitor cell transplantation in hearts with postinfarction left ventricular remodeling. Circulation 2007;115(14):1866–75.
[46] Sinha K, Das J, Pal PB, Sil PC. Oxidative stress: the mitochondria-dependent and mitochondria-independent pathways of apoptosis. Arch Toxicol 2013;87(7):1157–80.
[47] Li C, Li M, Chen P, Narayan S, Matschinsky FM, Bennett MJ, et al. Green tea polyphenols control dysregulated glutamate dehydrogenase in transgenic mice by hijacking the ADP activation site. J Biol Chem 2011;286(39):34164–74.